Electromagnetic Full Wave Modal Analysis of Frequency-Dependent Underground Cables

by

Md. Shahnoor Habib

A Thesis Submitted to the Faculty of Graduate Studies
in Partial Fulfillment of the Requirements for the
Degree of Masters of Science

Department of Electrical and Computer Engineering
University of Manitoba
Winnipeg, Manitoba, Canada

Acknowledgment

First and foremost, I would like to thank my academic advisor, Dr. Behzad Kordi, for his direction, encouragement and also for both mental and financial support during my Masters program. He inspired me in different ways all along the program. Without his guidance, it would not be possible to end up with this thesis.

I would like to thank Dr. Siamak Bonyadi, Dr. Maryam Heshmatzadeh, and Anuradha Kariyawasam for their help in different parts of my thesis. I gratefully acknowledge help from Mohammad Qudrat-E-Maula and Jayanta K. Debnath for their support and encouragement.

I also thank Dr. David Swatek, Dr. Jeewantha De Silva and Dr. Jitendra Paliwal for serving as committee members and giving their valuable evaluation.

I would like to thank Government of Manitoba for their financial support as scholarship (MGS). Manitoba HVDC Research Centre kindly permitted to use their PSCAD beta version which helped a lot in my research work. I gratefully acknowledge their support.

Lastly, my warmest thanks to all my family members for their continuous mental support which leads me to the end of the program.

To my parents and my wife

ABSTRACT

In this thesis, a new method has been proposed for calculating the frequency-dependent parameters of underground cables. The method uses full wave formulation for calculating the modal electromagnetic fields and corresponding voltages and currents and then extracting frequency-dependent per unit length parameters of underground cables. The proposed method can be used for any cross-sectional shape of cables. Coaxial cables and sector shaped cables are studied in this thesis and the calculated per-unit-length parameters are compared with those obtained from PSCAD/EMTDC and other methods available in the literature. Parametric studies have been done to analyze the effect of different variables of the underground cable and ground. In this method, proximity and skin effect is taken into consideration. Time domain simulations using the parameters calculated by proposed method are also presented and compared with the results from other available tools.

TABLE OF CONTENTS

LIST OF FIGURES

LIST OF TABLES

1. BACKGROUND

1.1 Introduction

Analysis of transmission lines is one of the important topics in power system analysis. The term Transmission Line (TL) is referred to both overhead line and underground cables. The dominant propagation mode of the transmission line is the transverse electromagnetic (TEM) mode. In TEM mode, the electric and magnetic fields surrounding the conductors stays in the transverse plane orthogonal to the line axis. At higher frequencies, higher order modes can coexist with this mode. The electromagnetic fields can interact with adjacent wires and can induces signal to those. This is termed as *crosstalk*. Transmission line model is very important to predict this kind of interaction. Now-a-days the analysis draws more attention as it can be used for the computation of the propagation characteristics of waveguides, antennas, printed circuits, high-speed interconnects, microstrip lines with many other applications in VLSI, MMICs, etc.

In most of early studies, the line parameters were calculated assuming low fre-

quency conditions. At low frequencies, the transmission line current is reasonably assumed to be distributed uniformly across the whole conductor. So, frequency-dependent effects such as skin effect and proximity were not considered. This assumption results in simpler formulations. However, in real life, accurate simulation of fast transients require consideration of the frequency dependence of the line parameters. Skin effect and proximity consideration take an important place in proper modeling of transmission line. Proximity is relatively more severe in cables as the conductors are more closely bounded compared to overhead lines. In overhead transmission lines the conductors are placed at a considerable distance from each other. So simplified assumption can be made by neglecting some mutual effect of the conductors on each other. Also, the conductors are placed far above the ground. But in underground cables, all the conductors are very closely bound and the cables are placed inside the ground. As a result, modeling becomes more complex in the case of underground cable.

Most simulation methods for underground cable as in [1], [3], [4], [5], [6], [7] are reasonably valid at power frequencies; however, they become inaccurate at higher frequencies. Further, measurements on cable systems show that the proximity effect strongly influences the wave propagation in cable systems, and commonly-used models are incapable of reproducing measurement results. In [8], [9], [10], [11] and [12], it is shown that simulation results are not consistent with measurements

for the inter-sheath mode excitation of a cable system.

First, we need to get an idea why cable is necessary when we have a simpler alternative like overhead line.

1.1.1 Advantages of Underground Cables

Underground cables are becoming more and more important in power system transmission and distribution, especially in the distribution network in urban area. In cities, overhead transmission lines are not very suitable as they create visual impact, connection difficulties, expansion problems, etc. Underground cables are becoming more popular in this case when all the technical, environmental and economic issues are considered.

With the advancement in technology, recent underground cables have several advantages compared to overhead lines as follow:

- Underground systems have longer lifetime than overhead lines [13],
- The maintenance costs are much lower,
- Underground cables are far less interrupted by bad weather like storm, snow, lightning, and strong wind,

- The transmission loss is lower [13],
- The electromagnetic radiation from cables to the surrounding is much lower than overhead lines,
- Use of land is conserved which is very important specially in city areas,
- Chances of accidents are reduced as the cables are less accessible,
- There are no noise or air pollution due to corona discharges, and,
- Obstacles like poles of overhead lines can be avoided which enhance the safety and beautification measurement in the city area.

1.1.2 Transients in Transmission Lines

Both the overhead lines and underground cables can be subject to transient over voltages or over currents. The origin of transients can be lighting strokes, switching operations, or some other sources. The transients can reach their peak very fast and can have different arbitrary waveforms. Transient signals usually contain a wide range of frequencies. In order to design the protective devices for the lines, the behavior of the system should be accurately described and predicted under these unusual situations. As a result, a transmission line model, which is valid for a wide range of frequencies, is so important.

Transmission line equations were mainly solved in the frequency domain in early transmission line simulation works. There were no direct time domain solution available theoretically except for some very simplified cases. But without the time domain simulations, the handling and operation of different nonlinear elements like thyristor, transformer, circuit breaker etc. would be difficult.

1.1.3 Importance of Frequency Dependent Model

Normal power is supplied at very low frequency mostly around 50 or 60 Hz. Simple transmission line models can be used only for this range of frequencies. Though there might be some issues with power quality such as resonances in electric facilities, effects of non-sinusoidal voltage supply, harmonic penetrations, etc. In general, those kind of issues are involved with frequencies up to few kHz [14]. The problem arises when transients are introduced in the line. Transients are surges or spikes or momentary changes in voltage and current which last for a short period of time. As mentioned before, there are various sources for transients like: lightning, switching operation on power lines, capacitor banks or even loads, loose or faulty connection, accidents by animals or human.

According to [15], [16], [17], [18], the frequency of the transients can be up to several MHz. These occur in a short period of time but still they need to be

analyzed as these high voltages or high currents can create considerable stress on insulation systems and other equipments like transformers and circuit breakers. Theoretically, circuit parameters are frequency dependent at all frequencies except DC. At lower frequency operation, approximation of fixed circuit parameters results in very negligible difference. But, at very high frequencies, frequency dependence can not be neglected any more because skin effect and proximity effect become important at those frequencies. We cannot use constant values for these circuit parameters because that will lead to considerable errors.

Therefore frequency independent models cannot be used to accurately calculate and predict the effect of these signals that have high-frequency contents and there is need for frequency-dependent transmission line modeling.

1.1.4 Skin Effect

Skin effect becomes important when non-DC (AC or transient) currents are analyzed. The DC currents flow through the whole cross section of the conductor. So if the cross sectional area of the conductor is doubled, the DC resistance per unit length will be half of the previous resistance. But for AC current, it is not that simple. AC currents tend to be distributed in a conductor in such a way that the current density near the surface is more than that at the center. That means AC currents tends to flow near the surface of the conductors. This effect is called “Skin

Effect". Skin depth is the average depth where most of the currents flow. It is defined as the depth below the surface of the conductors where the current density is reduced to *1/e* of the current density at the surface. Here, e is a mathematical constant, which is sometimes called $Euller's Number$. The approximate value of e is 2.71828. The equation for skin depth δ is [18],

$$\delta = \sqrt{\frac{2\rho}{\omega\mu}}, \tag{1.1}$$

where, ρ is the resistivity of the conductor, ω is the angular frequency of current, and μ is the magnetic permeability of the conductor.

For example, at 60 Hz the skin depth is 8.5 mm in copper. But at 100 kHz the skin depth is 0.208 mm and the effective resistance will be increased accordingly. That's why skin depth needs important consideration when high frequency signals, or transients are analyzed.

1.1.5 Proximity Effect

The AC current distribution in a conductor is also affected by the time-varying magnetic field produced by the current flowing in any adjacent conductor. The magnetic flux induces eddy currents in adjacent conductors and alters the overall distribution of currents flowing through them. As a result, the distribution of cur-

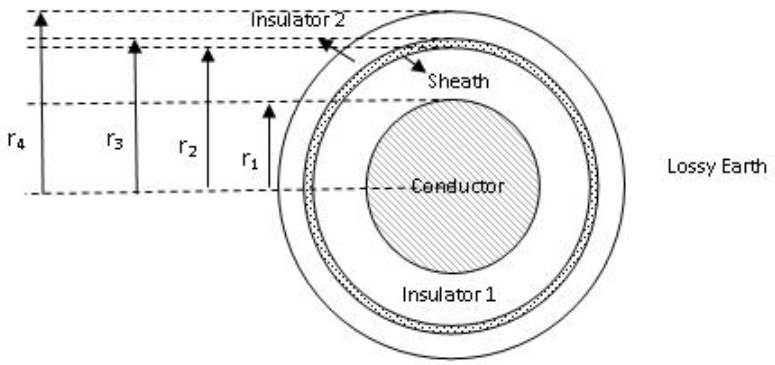

Fig. 1.1: Cable dimensions for the mathematical model introduced by Wedepohl [1]

rents within conductors will be forced to flow in a smaller region. This effect is called the proximity effect.

This effect can significantly increase the effective resistance and inductance of all the adjacent conductors. The effect will be greater if the distance between conductors is less and the frequency is high. In underground cable, the conductors are very close. So proximity effect can be very important for high frequency transient analysis.

1.2 Underground Cable Line Parameter Calculation

A detailed mathematical model was introduced by Wedepohl [1] for the calculation of impedance and admittance matrix for coaxial underground cable system. Skin effect was included in the model. The dimensions of single cable, used by Wedepohl, is given in Fig. 1.1. According to this model, the shunt admittance

submatrix for i^{th} cable is as follow,

$$Y_i = \begin{bmatrix} y_1 & -y_1 \\ -y_1 & y_1 + y_2 \end{bmatrix}, \tag{1.2}$$

where,

$$y_1 = g_1 + \frac{j\omega 2\pi\varepsilon_1}{\ln\left(\frac{r_2}{r_1}\right)}, \tag{1.3}$$

$$y_2 = g_2 + \frac{j\omega 2\pi\varepsilon_2}{\ln\left(\frac{r_4}{r_3}\right)}. \tag{1.4}$$

Here, g_1 and g_2 are the leakage conductances of the inner and outer insulations, ε_1 and ε_2 are their permittivities respectively.

If there are N cables, this submatrices can be placed as shown below to form the admittance matrix Y:

$$Y = \begin{bmatrix} Y_1 & 0 & 0 & . \\ 0 & Y_2 & 0 & . \\ 0 & 0 & Y_3 & . \\ . & . & . & . \end{bmatrix}. \tag{1.5}$$

For the impedance submatrix for each cable, there are seven components [1]. z_1, z_3 and z_5 are the internal impedances of the inner conductor, inner sheath and outer sheath respectively. z_2 and z_6 are the impedance due to time-varying magnetic field in the inner and outer insulation respectively. z_4 is the sheath mutual impedance and z_7 is the self impedance of the earth return path. The

formulation for all these components are as follow [1],

$$z_1 = \frac{\rho m}{2\pi r_1} \coth\left(0.777 m r_1\right) + \frac{0.356\rho}{\pi r_1^2}, \tag{1.6}$$

$$z_2 = \frac{j\omega\mu_1}{2} \ln\left(\frac{r_2}{r_1}\right), \tag{1.7}$$

$$z_3 = \frac{\rho m}{2\pi r_2} \coth\left(m\Delta\right) - \frac{\rho}{2\pi r_2\left(r_2 + r_3\right)}, \tag{1.8}$$

$$z_4 = \frac{\rho m}{\pi\left(r_2 + r_3\right)} \cos ech\left(m\Delta\right), \tag{1.9}$$

$$z_5 = \frac{\rho m}{2\pi r_3} \coth\left(m\Delta\right) + \frac{\rho}{2\pi r_3\left(r_2 + r_3\right)}, \tag{1.10}$$

$$z_6 = \frac{j\omega\mu_2}{2} \ln\left(\frac{r_4}{r_3}\right), \tag{1.11}$$

$$z_7 = \frac{j\omega\mu}{2\pi}\left\{-\ln\left(\frac{\gamma m r_4}{2}\right) + \frac{1}{2} - \frac{4mh}{3}\right\}, \tag{1.12}$$

where, ω is the angular frequency, ρ is the resistivity, γ is the Euler's constant, h is the burial depth of the cable, $m = \sqrt{\left(\frac{j\omega\mu}{\rho}\right)}$, $\Delta = r_3 - r_2$, μ_1 and μ_2 are the magnetic permeability of the inner and outer insulation respectively.

Now the impedance submatrix for single cable will be,

$$Z_i = \begin{bmatrix} z_1 + z_2 + z_3 + z_5 + z_6 + z_7 - 2z_4 & z_5 + z_6 + z_7 - z_4 \\ z_5 + z_6 + z_7 - z_4 & z_5 + z_6 + z_7 \end{bmatrix}. \tag{1.13}$$

The Z matrix for N cable system can be formed using the following equation,

$$Z = \begin{bmatrix} Z_1 & Z_{12} & Z_{13} & . \\ Z_{21} & Z_2 & Z_{23} & . \\ Z_{31} & Z_{32} & Z_3 & . \\ . & . & . & . \end{bmatrix}. \tag{1.14}$$

Here,

$$Z_{ji} = \begin{bmatrix} z_{ji} & z_{ji} \\ z_{ji} & z_{ji} \end{bmatrix}, \tag{1.15}$$

$$z_{ji} = \frac{j\omega\mu_g}{2\pi}\left\{-\ln\left(\frac{\gamma m s_{ji}}{2}\right) + \frac{1}{2} - \frac{2}{3}ml\right\}, \tag{1.16}$$

where, s_{ji} is the distance between the i_{th} and j_{th} cables, μ_g is the permeability of soil and l is the sum of the depths of the i_{th} and j_{th} cables. But this equation is limited by the condition $|ms_{ji}| < 0.25$. That means this formula is valid up to frequencies of the order of 100kHz [1]. PSCAD uses the modified version of these equations for underground cable modelling.

The impedance calculation for earth return path (1.12) is limited by the condition $|mr_4| < 0.25$. For cable parameter calculation, formulation for ground impedance can make considerable difference. Many research works have been done to improve the formulation, which are reviewed in the following section.

Ametani [19] extended the calculation of impedance and admittance matrix for the pipe type cable which has the core, sheath and armor. Both the model assumed that the displacement current is negligible in multiconductor system. Later Ametani introduced a new method [20] for calculating the impedances and admittances of multiconductors with arbitrary shaped cross sections. In this method, each arbitrary shaped conductor system is represented by a set of equivalent cylindrical conductors. Then the impedances and admittances are calculated by the previous method [19]. So, this method also have all the disadvantages of the Wedepohl method.

Similar subdivision technique is used in [21]. The shape of the subconductor can be square, circular or elemental. If circular or square sub-conductor is used, it requires a large number of subdivisions to achieve accurate results. But more computation and memory is required for those [22]. Lucas shows that elemental sub-conductor technique requires less number of subdivisions to get accurate results [22]. In [20], cable impedances was calculated only. In [23], simplified equations were presented to calculate capacitances of sector shaped cable approximately which was modified and used in [24] to calculate the capacitance of the sector shaped cable when it is buried inside the ground. But the components of the capacitance matrices are fixed and change in frequency does not change the values.

There are several literatures ([25], [26], [27], and [28]), where Finite Element Method (FEM) has been used for cable parameters calculation. But capacitance is not calculated in any of those. Also proximity effect was not addressed in details.

1.3 Inclusion of Ground Effects

For transmission line analysis, the effect of ground is very important. It is normally included by ground impedance and ground admittance. Some of the models for ground effect are accurate at low frequencies but diverge at higher frequencies. Some models give better results in a wide range of frequencies.

The ground impedance for buried cable was first developed by Pollaczek [29] for low frequencies. Here, the limitation for the frequencies was set by the condition $\omega \ll \sigma_g.\varepsilon_g^{-1}$. Here, σ_g is the ground conductivity and ε_g is the ground permittivity and ω is angular frequency of the signal. Pollaczek's formulation was complex for numerical solution. Later, Saad [30] derived equation which can approximate Pollaczek's expression,

$$Z_g = \frac{j\omega\mu_0}{2\pi}\left(K_0\left(\gamma_g^{'}R_{ab}\right) + \frac{2e^{-2d\gamma_g^{'}}}{4 + R_{ab}^2\left(\gamma_g^{'}\right)^2}\right). \tag{1.17}$$

Here, $K_0(.)$ is the Bessel's function of second kind and order zero, R_{ab} is the ex-

ternal radius of the wire for which the ground impedance is being calculated, and d is the burial depth of the cable.

It is also shown in [30] that above equation is a better approximation compared with the approximation proposed by Wedepohl [1]. Sunde [31] developed another approximation for a wide frequency range without the low frequency approximation (1.18),

$$Z_g = \frac{j\omega\mu_0}{2\pi}\left(K_0\left(\gamma_g R_{ab}\right) - K_0\left(\gamma_g\sqrt{R_{ab}^2+4d^2}\right) + 2\int_0^\infty \frac{e^{-2d\sqrt{\gamma_g^2+\lambda^2}}\cos\left(\lambda R_{ab}\right)}{\lambda+\sqrt{\gamma_g^2+\lambda^2}}d\lambda\right). \tag{1.18}$$

The problem with the equations is that integral term convergence takes longer time as the frequency increases and also causes truncation errors. Again, the first two Bessel terms becomes oscillatory when frequencies approach 1 MHz [32]. Wait [33] proposed exact expressions derived from rigorous electromagnetic theory. The frequency limit for the expression is set by the condition $\sqrt{\varepsilon_0\mu_0\omega^2} \ll 1$,

$$\begin{aligned} Z_g &= \tfrac{j\omega\mu_0}{2\pi}\left(1+\Delta\right)\ln\left(\tfrac{-j1.12}{\kappa R_{ab}}\right) \\ \kappa &= \sqrt{\varepsilon_g\mu_0\omega^2 - j\omega\mu_0\sigma_g}, \\ \varsigma &= 2j\kappa d, \\ \Delta &= \tfrac{1}{K_0(j\kappa R_{ab})}\begin{bmatrix} K_0\left(\varsigma\right)+\frac{2}{\varsigma}K_1\left(\varsigma\right), \\ -\frac{2}{\varsigma^2}+\left(1+\varsigma\right)e^{-\varsigma} \end{bmatrix}. \end{aligned} \tag{1.19}$$

Then Petrache [34] proposed a simple logarithmic approximation for the ground impedance as follow:

$$Z_g = \frac{j\omega\mu_0}{2\pi} \ln\left(\frac{1+\gamma_g R_{ab}}{\gamma_g R_{ab}}\right). \tag{1.20}$$

But this approximation does not take the cable burial depth into consideration which may lead to error in result. Theethayi [35] proposed a modified version of the empirical logarithmic-exponential equations to include the effect of burial depth as follow,

$$Z_g = \frac{j\omega\mu_0}{2\pi} \ln\left(\frac{1+\gamma_g R_{ab}}{\gamma_g R_{ab}}\right) + \left(\frac{2e^{-2d|\gamma_g|}}{4+\gamma_g^2 R_{ab}^2}\right). \tag{1.21}$$

In [32], it is shown that the last expression is both accurate and computationally efficient for a wide range of frequencies. But low frequency approximations of the ground impedance in conjunction with high resistivity soils is not appropriate for transient analysis.

1.4 Research Objective

The principle objective of this research was to calculate per unit length underground cable parameters for high frequency operation. Proximity effect and skin effect was taken into account in the frequency dependent parameter modeling. For this calculation, full wave electromagnetic equations was solved using Finite Element Method (FEM) for two dimensional system.

The other goal was to use these parameters in EMTP-like program to get time domain simulation and compare the results from available analytic solutions.

1.5 Contribution

In this thesis, we have shown the difference between the results from analytic formulation and our method both in frequency domain and time domain. The important thing about our method is its flexibility to use for any shape of cable system with even a large number of conductors. We have included the displacement currents for the ground which can be very vital at high frequency operations. Results from this method can be used as high frequency bench mark.

We have also done some parametric studies which shows the effect of some important parameter like cable burial depth, ground conductivity, wire conductivity etc. on per unit length impedance and admittance of the cable system. Modeling of a sector shaped cable system was also performed using full wave method which is not yet available using EMTP-like programs.

1.6 Thesis Outline

In chapter 1, we discussed the background of the cable parameter calculation. In chapter 2, electromagnetic theory related to the transmission line modeling is discussed. In the first part, the formulation of modal analysis is given. Here, we discussed about the similarity transformation matrix and how it is used for phase domain to mode domain conversion. In the second part, full wave theory is reviewed. Maxwell's equations, difference between full wave and quasi-static formulation, and the boundary conditions between two medium is also addressed. At last we explained the process of calculation the circuit parameters of a transmission line from the electromagnetic parameters.

The method used in this thesis is discussed in the first part of chapter 3. We demonstrated the calculation for a two conductor transmission line. Same process can be extended for n number of conductors. We used data from PSCAD to compare the results from our method. In the last part of chapter 3, we explained how PSCAD data was used for comparison.

In chapter 4, we demonstrate several cases with single cable with single conductor, single cable with conductor and sheath, two cables, three cables, and sector shaped cable. We studied the effect of changing some of parameters like cable burial depth, ground conductivity, ground permittivity, conductor conductivity, conductor permittivity, and distance between two cable. At the end of the chap-

ter, we showed an example where it is clearly shown that proximity effect is taken into account during the calculation using our method.

In chapter 5, time domain simulation is shown. Here we again used PSCAD for comparing our results.

In chapter 6, we have given our conclusion remarks. We also discussed about the scope for future works.

2. THEORY

2.1 Modal Analysis

In this section, it is assumed that the time variation of the source is sinusoidal and the transmission line is in steady state. Therefore, the line voltages and currents are also sinusoidal having a magnitude and a phase angle. Thus, we denote the line voltages and line currents in their phasor forms,

$$V_i(z,t) = \mathrm{Re}\{\hat{V}_i(z)e^{j\omega t}\}, \tag{2.1}$$

$$I_i(z,t) = \mathrm{Re}\{\hat{I}_i(z)e^{j\omega t}\}. \tag{2.2}$$

The time domain forms of the line voltages and currents are,

$$V_i(z,t) = \left|\hat{V}_i(z)\right| \cos(\omega t + \angle\hat{V}_i(z)), \tag{2.3}$$

$$I_i(z,t) = \left|\hat{I}_i(z)\right| \cos(\omega t + \angle\hat{I}_i(z)). \tag{2.4}$$

The MTL equations for sinusoidal, steady-state excitation can be written in

phasor forms as,

$$\frac{d}{dz}\hat{\boldsymbol{V}}(z) = -\hat{\boldsymbol{Z}}\hat{\boldsymbol{I}}(z), \tag{2.5}$$

$$\frac{d}{dz}\hat{\boldsymbol{I}}(z) = -\hat{\boldsymbol{Y}}\hat{\boldsymbol{V}}(z), \tag{2.6}$$

where, the per unit length impedance matrix $\hat{\boldsymbol{Z}}$ and admittance matrix $\hat{\boldsymbol{Y}}$ are given by:

$$\hat{\boldsymbol{Z}} = \boldsymbol{R} + j\omega\boldsymbol{L}, \tag{2.7}$$

$$\hat{\boldsymbol{Y}} = \boldsymbol{G} + j\omega\boldsymbol{C}. \tag{2.8}$$

Here, the **R**, **L**, **G** and **C** are the per unit length resistance, inductance, conductance and capacitance respectively. All these matrices are assumed to be independent of frequency, however, in the general case they can be functions of frequency. This set of coupled first order ordinary differential equations can be put in the matrix form as follows,

$$\frac{d}{dz}\begin{bmatrix} \hat{\boldsymbol{V}}(z) \\ \hat{\boldsymbol{I}}(z) \end{bmatrix} = \begin{bmatrix} 0 & -\hat{\boldsymbol{Z}} \\ -\hat{\boldsymbol{Y}} & 0 \end{bmatrix}\begin{bmatrix} \hat{\boldsymbol{V}}(z) \\ \hat{\boldsymbol{I}}(z) \end{bmatrix}. \tag{2.9}$$

For an $(n+1)$ conductor transmission line, **R**, **L**, **G**, **C**, $\hat{\boldsymbol{Z}}$ and $\hat{\boldsymbol{Y}}$ are $n \times n$ matrix and $\hat{\boldsymbol{V}}$ and $\hat{\boldsymbol{I}}$ are $n \times 1$ vectors.

2.1.1 Phase Domain to Mode Domain Conversion

The equations for $\hat{\boldsymbol{V}}$ and $\hat{\boldsymbol{I}}$ are coupled first order differential equations. These equations need to be solved incorporating the terminal constraints which contain the lumped voltage and current source excitation and also the load impedance of the line. One method for solving these equations is by decoupling the MTL equations using similarity transformations [18]. In this technique, two new parameters in the mode domain are introduced which will be denoted as the mode voltage $\hat{\boldsymbol{V}}_{\boldsymbol{m}}(z)$ and the mode current $\hat{\boldsymbol{I}}_{\boldsymbol{m}}(z)$ vectors. These new variables are defined as follows,

$$\hat{\boldsymbol{V}}(z) = \hat{\boldsymbol{T}}_{\boldsymbol{V}} \hat{\boldsymbol{V}}_{\boldsymbol{m}}(z), \tag{2.10}$$

$$\hat{\boldsymbol{I}}(z) = \hat{\boldsymbol{T}}_{\boldsymbol{I}} \hat{\boldsymbol{I}}_{\boldsymbol{m}}(z). \tag{2.11}$$

Here, $\hat{\boldsymbol{T}}_{\boldsymbol{I}}$ and $\hat{\boldsymbol{T}}_{\boldsymbol{V}}$ are called the similarity transformation matrices. The matrices have dimensions of $n \times n$ and can be complex. To make above transformation between the mode domain voltages and currents and the phase domain voltages and currents valid, $\hat{\boldsymbol{T}}_{\boldsymbol{I}}$ and $\hat{\boldsymbol{T}}_{\boldsymbol{V}}$ must be nonsingular which means that $\hat{\boldsymbol{T}}_{\boldsymbol{I}}^{-1}$ and $\hat{\boldsymbol{T}}_{\boldsymbol{V}}^{-1}$ must exist.

By applying these equations to the matrix from of MTL equations (2.9), we

have,

$$\frac{d}{dz}\begin{bmatrix} \hat{\boldsymbol{V}}_{\boldsymbol{m}}(z) \\ \hat{\boldsymbol{I}}_{\boldsymbol{m}}(z) \end{bmatrix} = \begin{bmatrix} 0 & -\hat{\boldsymbol{T}}_{\boldsymbol{V}}^{-1}\hat{\boldsymbol{Z}}\hat{\boldsymbol{T}}_{\boldsymbol{I}} \\ -\hat{\boldsymbol{T}}_{\boldsymbol{I}}^{-1}\hat{\boldsymbol{Y}}\hat{\boldsymbol{T}}_{\boldsymbol{V}} & 0 \end{bmatrix} \begin{bmatrix} \hat{\boldsymbol{V}}_{\boldsymbol{m}}(z) \\ \hat{\boldsymbol{I}}_{\boldsymbol{m}}(z) \end{bmatrix}. \tag{2.12}$$

The MTL equations can be decoupled if $\hat{\boldsymbol{T}}_{\boldsymbol{I}}$ and $\hat{\boldsymbol{T}}_{\boldsymbol{V}}$ can diagonalize $\hat{\boldsymbol{Z}}$ and $\hat{\boldsymbol{Y}}$ separately. In other words,

$$\begin{aligned} &\hat{\boldsymbol{T}}_{\boldsymbol{V}}^{-1}\hat{\boldsymbol{Z}}\hat{\boldsymbol{T}}_{\boldsymbol{I}} = \hat{\boldsymbol{z}} \\ &= \begin{bmatrix} \hat{z}_1 & 0 & \cdots & 0 \\ 0 & \hat{z}_2 & \ddots & \vdots \\ \vdots & \ddots & \ddots & 0 \\ 0 & \cdots & 0 & \hat{z}_n \end{bmatrix}, \end{aligned} \tag{2.13}$$

$$\begin{aligned} &\hat{\boldsymbol{T}}_{\boldsymbol{I}}^{-1}\hat{\boldsymbol{Y}}\hat{\boldsymbol{T}}_{\boldsymbol{V}} = \hat{\boldsymbol{y}} \\ &= \begin{bmatrix} \hat{y}_1 & 0 & \cdots & 0 \\ 0 & \hat{y}_2 & \ddots & \vdots \\ \vdots & \ddots & \ddots & 0 \\ 0 & \cdots & 0 & \hat{y}_n \end{bmatrix}. \end{aligned} \tag{2.14}$$

Then the phasor decoupled MTL equations will be as follows,

$$\frac{d}{dz}\begin{bmatrix} \hat{V}_{m1}(z) \\ \hat{V}_{m2}(z) \\ \vdots \\ \hat{V}_{mn}(z) \end{bmatrix} = -\begin{bmatrix} \hat{z}_1 & 0 & \cdots & 0 \\ 0 & \hat{z}_2 & \ddots & \vdots \\ \vdots & \ddots & \ddots & 0 \\ 0 & \cdots & 0 & \hat{z}_n \end{bmatrix}\begin{bmatrix} \hat{I}_{m1}(z) \\ \hat{I}_{m2}(z) \\ \vdots \\ \hat{I}_{mn}(z) \end{bmatrix}, \tag{2.15}$$

$$\frac{d}{dz}\begin{bmatrix} \hat{I}_{m1}(z) \\ \hat{I}_{m2}(z) \\ \vdots \\ \hat{I}_{mn}(z) \end{bmatrix} = -\begin{bmatrix} \hat{y}_1 & 0 & \cdots & 0 \\ 0 & \hat{y}_2 & \ddots & \vdots \\ \vdots & \ddots & \ddots & 0 \\ 0 & \cdots & 0 & \hat{y}_n \end{bmatrix}\begin{bmatrix} \hat{V}_{m1}(z) \\ \hat{V}_{m2}(z) \\ \vdots \\ \hat{V}_{mn}(z) \end{bmatrix}. \tag{2.16}$$

Now if two $n \times n$ matrices $\hat{\boldsymbol{T}}_{\boldsymbol{I}}$ and $\hat{\boldsymbol{T}}_{\boldsymbol{V}}$ can be found which simultaneously diagonalize both $\hat{\boldsymbol{Z}}$ and $\hat{\boldsymbol{Y}}$ then the solution of n coupled equations can be reduced to n decoupled equations. Since, $\hat{\boldsymbol{Z}}$ and $\hat{\boldsymbol{Y}}$ are symmetric then according to [18],

$$\hat{\boldsymbol{T}}_{\boldsymbol{I}}^{t} = \hat{\boldsymbol{T}}_{\boldsymbol{V}}^{-1}. \tag{2.17}$$

The two sets of coupled equations can be used to form one second order uncoupled set of equations. The second order uncoupled set of equations can be in terms of voltage $\hat{\boldsymbol{V}}$ or current $\hat{\boldsymbol{I}}$. The uncoupled, second-order MTL equations are,

$$\frac{d^2}{dz^2}\hat{\boldsymbol{V}}(z) = \hat{\boldsymbol{Z}}\hat{\boldsymbol{Y}}\hat{\boldsymbol{V}}(z), \tag{2.18}$$

$$\frac{d^2}{dz^2}\hat{\boldsymbol{I}}(z) = \hat{\boldsymbol{Y}}\hat{\boldsymbol{Z}}\hat{\boldsymbol{I}}(z). \tag{2.19}$$

Substitution of similarity transformation in (2.19) yields,

$$\begin{aligned} \tfrac{d^2}{dz^2}\hat{\boldsymbol{I}}_{\boldsymbol{m}}(z) &= \hat{\boldsymbol{T}}_{\boldsymbol{I}}^{-1}\hat{\boldsymbol{Y}}\hat{\boldsymbol{Z}}\hat{\boldsymbol{T}}_{\boldsymbol{I}}\hat{\boldsymbol{I}}_{\boldsymbol{m}}(z), \\ &= \hat{\boldsymbol{T}}_{\boldsymbol{I}}^{-1}\hat{\boldsymbol{Y}}\hat{\boldsymbol{T}}_{\boldsymbol{V}}\hat{\boldsymbol{T}}_{\boldsymbol{V}}^{-1}\hat{\boldsymbol{Z}}\hat{\boldsymbol{T}}_{\boldsymbol{I}}\hat{\boldsymbol{I}}_{\boldsymbol{m}}(z), \\ &= \hat{\boldsymbol{y}}\hat{\boldsymbol{z}}\hat{\boldsymbol{I}}_{\boldsymbol{m}}(z). \end{aligned} \tag{2.20}$$

If we choose

$$\hat{\boldsymbol{T}}_{\boldsymbol{I}} = \hat{\boldsymbol{T}}, \tag{2.21}$$

then,

$$\hat{\boldsymbol{T}}_{\boldsymbol{V}} = \hat{\boldsymbol{T}}_{-1}^{t}, \tag{2.22}$$

and, the equations will become,

$$\begin{aligned} \tfrac{d^2}{dz^2}\hat{\boldsymbol{I}}_{\boldsymbol{m}}(z) &= \hat{\boldsymbol{T}}^{-1}\hat{\boldsymbol{Y}}\hat{\boldsymbol{Z}}\hat{\boldsymbol{T}}\hat{\boldsymbol{I}}_{\boldsymbol{m}}(z) \\ &= \hat{\gamma}^2\hat{\boldsymbol{I}}_{\boldsymbol{m}}(z). \end{aligned} \tag{2.23}$$

Here, $\boldsymbol{\gamma}^2$ is a diagonal matrix as,

$$\hat{\boldsymbol{\gamma}}^2 = \begin{bmatrix} \hat{\gamma}_1^2 & 0 & \cdots & 0 \\ 0 & \hat{\gamma}_2^2 & \ddots & \vdots \\ \vdots & \ddots & \ddots & 0 \\ 0 & \cdots & 0 & \hat{\gamma}_n^2 \end{bmatrix}. \tag{2.24}$$

The general solution to the uncoupled equations in (2.23) is,

$$\hat{\boldsymbol{I}}_{\boldsymbol{m}}(z) = e^{-\hat{\boldsymbol{\gamma}}z}\hat{\boldsymbol{I}}_{\boldsymbol{m}}^{+} - e^{\hat{\boldsymbol{\gamma}}z}\hat{\boldsymbol{I}}_{\boldsymbol{m}}^{-}. \tag{2.25}$$

Here, the $e^{\pm\hat{\boldsymbol{\gamma}}z}$ are matrices and the matrix exponentials are defined as follow:

$$e^{\pm\hat{\boldsymbol{\gamma}}z} = \begin{bmatrix} e^{\pm\hat{\gamma}_1 z} & 0 & \cdots & 0 \\ 0 & e^{\pm\hat{\gamma}_2 z} & \ddots & \vdots \\ \vdots & \ddots & \ddots & 0 \\ 0 & \cdots & 0 & e^{\pm\hat{\gamma}_n z} \end{bmatrix}, \tag{2.26}$$

and, the modal currents are,

$$\hat{\boldsymbol{I}}_{\boldsymbol{m}}^{\pm} = \begin{bmatrix} I_{m1}^{\pm}(z) \\ I_{m2}^{\pm}(z) \\ \vdots \\ I_{mn}^{\pm}(z) \end{bmatrix}. \tag{2.27}$$

The line currents are given by,

$$\begin{aligned} \hat{\boldsymbol{I}}(z) &= \hat{\boldsymbol{T}}\hat{\boldsymbol{I}}_{\boldsymbol{m}}(z), \\ &= \hat{\boldsymbol{T}}(e^{-\hat{\gamma}z}\hat{\boldsymbol{I}}_{\boldsymbol{m}}^{+} - e^{\hat{\gamma}z}\hat{\boldsymbol{I}}_{\boldsymbol{m}}^{-}). \end{aligned} \tag{2.28}$$

Similarly, the solution for uncoupled mode voltages can be found from the other second order differential equation,

$$\begin{aligned} \tfrac{d^2}{dz^2}\hat{\boldsymbol{V}}_{\boldsymbol{m}}(z) &= \hat{\boldsymbol{T}}_{\boldsymbol{V}}^{-1}\hat{\boldsymbol{Z}}\hat{\boldsymbol{Y}}\hat{\boldsymbol{T}}_{\boldsymbol{V}}\hat{\boldsymbol{V}}_{\boldsymbol{m}}(z), \\ &= \hat{\boldsymbol{T}}^{t}\hat{\boldsymbol{Z}}\hat{\boldsymbol{Y}}(\hat{\boldsymbol{T}}^{t})^{-1}\hat{\boldsymbol{V}}_{\boldsymbol{m}}(z), \\ &= \hat{\gamma}^2\hat{\boldsymbol{V}}_{\boldsymbol{m}}(z). \end{aligned} \tag{2.29}$$

The modal voltages are solution of (2.29) given by,

$$\hat{\boldsymbol{V}}_{\boldsymbol{m}}(z) = e^{-\hat{\gamma}z}\hat{\boldsymbol{V}}_{\boldsymbol{m}}^{+} + e^{\hat{\gamma}z}\hat{\boldsymbol{V}}_{\boldsymbol{m}}^{-}. \tag{2.30}$$

The line voltages can be found from the mode voltages

$$\begin{aligned}\hat{\boldsymbol{V}}(z) &= \hat{\boldsymbol{T}}_{\boldsymbol{V}}\hat{\boldsymbol{V}}_{\boldsymbol{m}}(z),\\ &= (\hat{\boldsymbol{T}}^{-1})^{t}\hat{\boldsymbol{V}}_{\boldsymbol{m}}(z),\\ &= \hat{\boldsymbol{T}}(e^{-\hat{\gamma}z}\hat{\boldsymbol{V}}_{\boldsymbol{m}}^{+} + e^{\hat{\gamma}z}\hat{\boldsymbol{V}}_{\boldsymbol{m}}^{-}).\end{aligned} \tag{2.31}$$

2.2 Full Wave Electromagnetic Analysis

The simulations in Full Wave (FW) analysis are based on the solution of Maxwell's equations. The Maxwell's' equations in the frequency domain are given by,

$$\nabla \times \vec{\boldsymbol{E}} = -j\omega\vec{\boldsymbol{B}}, \tag{2.32}$$

$$\nabla \times \vec{\boldsymbol{H}} = \vec{\boldsymbol{J}} + j\omega\vec{\boldsymbol{D}}, \tag{2.33}$$

$$\nabla.\vec{\boldsymbol{D}} = \rho, \tag{2.34}$$

$$\nabla.\vec{\boldsymbol{B}} = 0, \tag{2.35}$$

where, $\vec{\boldsymbol{H}}$ is the magnetic field intensity, $\vec{\boldsymbol{E}}$ is the electric field intensity, $\vec{\boldsymbol{J}}$ is the current density, $\vec{\boldsymbol{D}}$ is the electric flux density, $\vec{\boldsymbol{B}}$ is the magnetic flux density, and ρ is the external electric charge density. If the region is free of external charge, then ρ will be zero in (2.34)

This set of equations, with the help of some other auxiliary relations and definition, governs all electromagnetic phenomenons where the frequency can vary from zero up to highest frequency of radio waves.

Some other auxiliary relations and definitions are,

- Conduction current: For a conductor with conductivity of σ and the electric field intensity of $\vec{\boldsymbol{E}}$, the conduction current density is given by,

$$\vec{\boldsymbol{J}} = \sigma \vec{\boldsymbol{E}}. \tag{2.36}$$

- Permittivity: The relation between the electric flux density $\vec{\boldsymbol{D}}$ and the electric field intensity $\vec{\boldsymbol{E}}$ is,

$$\vec{\boldsymbol{D}} = \varepsilon \vec{\boldsymbol{E}} = \varepsilon_r \varepsilon_0 \vec{\boldsymbol{E}}. \tag{2.37}$$

  Here, ε_0 represents the permittivity of free space whose value is 8.854×10^{-12}F/m. ε_r is the relative permittivity whose value depends on the material in the medium and takes account the effect of the atomic and molecular dipoles in the material.

- Permeability: The relation between the magnetic flux density $\vec{\boldsymbol{B}}$ and the magnetic field intensity $\vec{\boldsymbol{H}}$ is,

$$\vec{\boldsymbol{B}} = \mu \vec{\boldsymbol{H}} = \mu_r \mu_0 \vec{\boldsymbol{H}}. \tag{2.38}$$

Here, μ_0 is the permeability of free space and its value is $4\pi \times 10^{-7}$H/m and μ_r is the relative permeability of the material used as the medium. It characterizes the effect of the magnetic dipole moments of the medium.

Using the given relations, the Maxwell's equations can be rewritten for a charge free region as follow,

$$\nabla \times \vec{\boldsymbol{E}} = -j\omega\mu\vec{\boldsymbol{H}}, \tag{2.39}$$

$$\nabla \times \vec{\boldsymbol{H}} = (\sigma + j\omega\varepsilon)\vec{\boldsymbol{E}}, \tag{2.40}$$

$$\nabla.\vec{\boldsymbol{E}} = 0, \tag{2.41}$$

$$\nabla.\vec{\boldsymbol{H}} = 0. \tag{2.42}$$

In this thesis,we assume the electromagnetic fields propagate in the z direction. So, we can write:

$$\vec{\boldsymbol{E}}(x,y,z) = \vec{\hat{\boldsymbol{E}}}(x,y)e^{-\gamma z}, \tag{2.43}$$

$$\vec{\boldsymbol{H}}(x,y,z) = \vec{\hat{\boldsymbol{H}}}(x,y)e^{-\gamma z}, \tag{2.44}$$

or,

$$\vec{\boldsymbol{E}} = \underbrace{\hat{E}_x(x,y)e^{-\gamma z}}_{E_x}\hat{a}_x + \underbrace{\hat{E}_y(x,y)e^{-\gamma z}}_{E_y}\hat{a}_y + \underbrace{\hat{E}_z(x,y)e^{-\gamma z}}_{E_z}\hat{a}_z, \tag{2.45}$$

$$\vec{\boldsymbol{H}} = \underbrace{\hat{H}_x(x,y)e^{-\gamma z}}_{H_x}\hat{a}_x + \underbrace{\hat{H}_y(x,y)e^{-\gamma z}}_{H_y}\hat{a}_y + \underbrace{\hat{H}_z(x,y)e^{-\gamma z}}_{H_z}\hat{a}_z. \tag{2.46}$$

In (2.43) and (2.44), γ is the propagation constant. It can be represented as follow,

$$\gamma = \alpha + j\beta, \tag{2.47}$$

where, α is the attenuation constant, and β is the phase constant.

By using Maxwell four equations (2.39 - 2.42), we can derive the wave equation for a charge free region as follow,

$$\begin{aligned} &\nabla \times \nabla \times \vec{\boldsymbol{E}} = -j\omega\mu\nabla \times \vec{\boldsymbol{H}}, \\ &\nabla(\nabla.\vec{\boldsymbol{E}}) - \nabla^2\vec{\boldsymbol{E}} + j\omega\mu(\sigma + j\omega\varepsilon)\vec{\boldsymbol{E}} = 0, \\ &\nabla^2\vec{\boldsymbol{E}} + \underbrace{(\omega^2\mu\varepsilon - j\omega\mu\sigma)}_{k^2}\vec{\boldsymbol{E}} = 0. \end{aligned} \tag{2.48}$$

Using (2.45) for the x component of the electric field in (2.48), we get,

$$\begin{aligned} &\tfrac{\partial^2}{\partial x^2}E_x + \tfrac{\partial^2}{\partial y^2}E_x + \tfrac{\partial^2}{\partial z^2}E_x + k^2E_x = 0, \\ &\tfrac{\partial^2}{\partial x^2}E_x + \tfrac{\partial^2}{\partial y^2}E_x + \gamma^2E_x + k^2E_x = 0, \\ &\nabla_t^2E_x + (\gamma^2 + k^2)E_x = 0, \end{aligned} \tag{2.49}$$

where, $\nabla_t \triangleq \frac{\partial}{\partial x}\hat{a}_x + \frac{\partial}{\partial y}\hat{a}_y$.

Similarly, we can get,

$$\nabla_t^2E_y + (\gamma^2 + k^2)E_y = 0, \tag{2.50}$$

$$\nabla_t^2E_z + (\gamma^2 + k^2)E_z = 0. \tag{2.51}$$

Or,

$$\nabla_t^2 \vec{\boldsymbol{E}} + (\gamma^2 + k^2)\vec{\boldsymbol{E}} = 0. \tag{2.52}$$

This is a eigenvalue problem, which is solved using Finite Element Method (FEM). In this thesis, we have used Comsol Multiphysics, that is a commercial FEM solver.

2.2.1 Quasi-static vs. Full Wave Formulations

There are two sets of equations for solving common electromagnetic problems. They are referred to as quasi-static and full wave formulations. Major difference between these two is their functionality on structures of different electrical sizes. Electrical size represents the ratio between the largest distance between any two point of the structure and the smallest wavelength of the electromagnetic field. Quasi-static formulation is applicable for electrically small structures. In practice, quasi-static simulation is reasonable where the electrical size is smaller than $\frac{1}{10}$. For quasi-static cases, it is assumed that the currents and charges, which generate the electromagnetic field, are changing very slowly with respect to time. We know that the wavelength is given by,

$$\lambda = \frac{v}{f}, \tag{2.53}$$

$$\text{electric size} = \frac{d}{\lambda} = \frac{d \times f}{v}, \tag{2.54}$$

where, λ is the wavelength, v is the velocity of wave, f is frequency of the signal, and d is the largest distance between any two points of the structure.
If d and v are constant then f must be small to keep the electrical size smaller than $\frac{1}{10}$. So, in quasi-static simulation, there is limit for upper bound of the frequency range.

On the other hand, when the frequency is high, the variation in amount of charges changes rapidly with respect to time. So, full wave Maxwell equations application mode needs to be applied.
In general, quasi-static is a simplified version of full wave formulation which can be applied in some limited conditions.

2.2.2 Circuit Parameter Calculation

In transmission line theory, currents and voltages are used as circuit parameters. But in full wave analysis, we get the electric and magnetic fields only. A simple example of a single cable system with two conductors, buried inside the ground, (Fig. 2.1) is given here to demonstrate how, in this thesis, the electromagnetic parameters are used to calculate the circuit parameters.

First, we set a reference point for the voltage calculation. Then the following equations are used to calculate voltages and currents from electric field and current density. If the electric field along a particular line (Fig 2.1) of length l_i is $\vec{\boldsymbol{E}}$ then

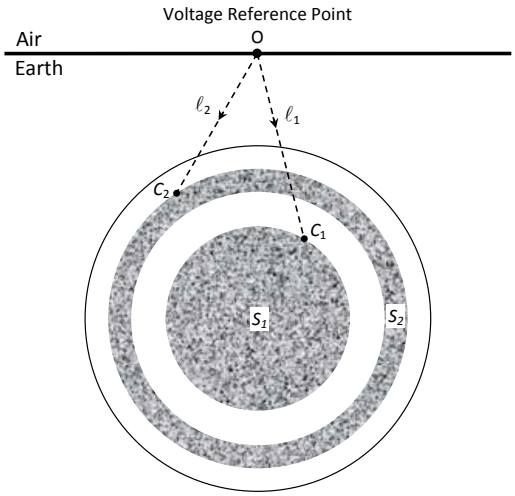

Fig. 2.1: Voltage can be calculated by integrating electric field $\vec{\boldsymbol{E}}$ across the line of length l_1 or l_2. Current can be calculated by integrating current density $\vec{\boldsymbol{J}}$ or $\sigma\vec{\boldsymbol{E}}$ across the cross section area S_1 or S_2.

the voltage drop V_i across the line would be:

$$V_i = -\int_O^{C_i} \vec{\boldsymbol{E}}.d\vec{\boldsymbol{l}}. \tag{2.55}$$

If a conductor (Fig 2.1) with cross section area of S_i and conductivity of σ_i has current density of $\vec{\boldsymbol{J}}$ along the direction normal to the cross section then the current flowing through the cross section will be:

$$I_i = \int_{S_i} \vec{\boldsymbol{J}}.d\boldsymbol{s} = \int_{S_i} J_z ds = \sigma \int_{S_i} E_z ds. \tag{2.56}$$

In (2.56), we assume the displacement current density $\frac{\partial}{\partial t}D$ is negligible, which is a valid approximation in good conductors.

3. FULL WAVE ANALYSIS OF TRANSMISSION LINE

3.1 Full Wave Calculation

The first order coupled phasor MTL equations for $n+1$ number of conductors, given in Chapter 2, are as follow,

$$\frac{d}{dz}\hat{\boldsymbol{V}}(z) = -\hat{\boldsymbol{Z}}\hat{\boldsymbol{I}}(z), \tag{3.1a}$$

$$\frac{d}{dz}\hat{\boldsymbol{I}}(z) = -\hat{\boldsymbol{Y}}\hat{\boldsymbol{V}}(z). \tag{3.1b}$$

In (3.1), $\hat{\boldsymbol{V}}$ is a $n \times 1$ vector of line voltages, and $\hat{\boldsymbol{I}}$ is the $n \times 1$ vector of line currents of transmission lines or cable system. $\hat{\boldsymbol{Z}}$ and $\hat{\boldsymbol{Y}}$ are $n \times n$ per unit length impedance and admittance matrices, respectively. In the modal excitation of the cable system, for each mode, the electromagnetic fields, and consequently, the line voltages and currents propagate with the same propagation constant. In other words, for each propagating mode we can write,

$$\hat{\boldsymbol{V}}(z) = \hat{\boldsymbol{V}}_m e^{-\gamma z}, \tag{3.2a}$$

$$\hat{\boldsymbol{I}}(z) = \hat{\boldsymbol{I}}_m e^{-\gamma z}. \tag{3.2b}$$

The $n \times 1$ vectors $\hat{\boldsymbol{V}}_{\boldsymbol{m}}$ and $\hat{\boldsymbol{I}}_{\boldsymbol{m}}$ in (3.2) are the modal line voltages and currents that are calculated by integrating the electromagnetic fields. In the case of 2D simulation of a 3D structure, the third dimension is assumed to be infinitely long. That makes the transmission line reflectionless. Substitution of (3.2) in (3.1) yields,

$$\gamma \hat{\boldsymbol{V}}_m = \hat{\boldsymbol{Z}} \hat{\boldsymbol{I}}_m, \tag{3.3a}$$

$$\gamma \hat{\boldsymbol{I}}_m = \hat{\boldsymbol{Y}} \hat{\boldsymbol{V}}_m, \tag{3.3b}$$

where, γ, $\hat{\boldsymbol{V}}_{\boldsymbol{m}}$ and $\hat{\boldsymbol{I}}_{\boldsymbol{m}}$ are known and have been determined using the full wave modal analysis of cable system.

Once we write (3.3) for all n propagating modes, we have a set of linear equations whose solution will provide us with the unknown per unit length impedance and admittance matrices. For example, for the case of a two conductor cable system, where we have two propagating modes, (3.3) can be written as,

$$\underbrace{\begin{bmatrix} \gamma^1 V_1^1 & \gamma^2 V_1^2 \\ \gamma^1 V_2^1 & \gamma^2 V_2^2 \end{bmatrix}}_{\boldsymbol{V}_\gamma} = \begin{bmatrix} Z_{11} & Z_{12} \\ Z_{21} & Z_{22} \end{bmatrix} \begin{bmatrix} I_1^1 & I_1^2 \\ I_2^1 & I_2^2 \end{bmatrix}, \tag{3.4a}$$

$$\underbrace{\begin{bmatrix} \gamma^1 I_1^1 & \gamma^2 I_1^2 \\ \gamma^1 I_2^1 & \gamma^2 I_2^2 \end{bmatrix}}_{\boldsymbol{I}_\gamma} = \begin{bmatrix} Y_{11} & Y_{12} \\ Y_{21} & Y_{22} \end{bmatrix} \begin{bmatrix} V_1^1 & V_1^2 \\ V_2^1 & V_2^2 \end{bmatrix}. \tag{3.4b}$$

.

In (3.4), γ^k represents propagation constant of the k^{th} mode, and V_i^k and I_i^k are the voltage and current of the i^{th} conductor for the k^{th} mode. The impedance and admittance matrices can be calculated using,

$$\begin{bmatrix} Z_{11} & Z_{12} \\ Z_{21} & Z_{22} \end{bmatrix} = \boldsymbol{V}_\gamma \begin{bmatrix} I_1^1 & I_1^2 \\ I_2^1 & I_2^2 \end{bmatrix}^{-1}, \tag{3.5a}$$

$$\begin{bmatrix} Y_{11} & Y_{12} \\ Y_{21} & Y_{22} \end{bmatrix} = \boldsymbol{I}_\gamma \begin{bmatrix} V_1^1 & V_1^2 \\ V_2^1 & V_2^2 \end{bmatrix}^{-1}. \tag{3.5b}$$

3.1.1 Finite Element Method

In this thesis, Comsol Multiphysics is used the for the full wave calculations. Comsol is a FEM based solution tool. Mode analysis, using the eigenvalue solver, gives the possible modes that can be obtained by simulating for different propagation constants. Fig. 3.1 shows the flow chart of the whole process followed for full wave calculation.

We need a finite area for the simulation using FEM. Circular truncation boundary (Fig. 3.2) was selected to limit the solution area. The size of the boundary de-

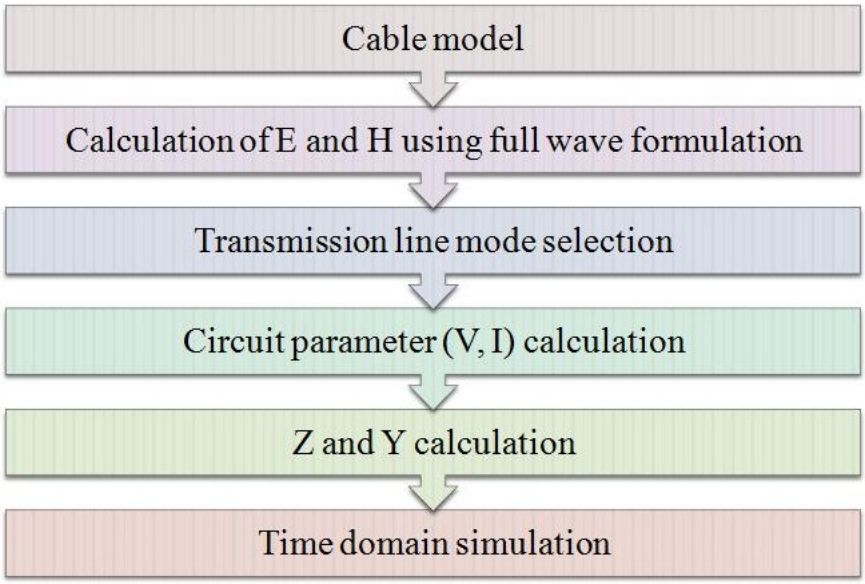

Fig. 3.1: Flow chart for the full wave method for calculating pur unit length underground cable parameters.

pends on the operating frequency. It also depends on the conductivity and relative permeability of the ground. When ground carry the return current, the penetration depth δ inside the ground can be calculated using $\delta = \sqrt{\frac{2\rho}{\omega\mu}}$. Here, ω is the operating angular frequency, ρ is the resistivity of the ground and μ is the relative permeability of the ground. We selected the radius of the the truncation boundary much larger than this penetration depth. For the truncation boundary, the boundary condition was zero current. For other boundaries in the whole model, the condition was continuity.

For cables buried in lossy earth, there are many choices for the selection of the reference point. One can choose a point too far from the cable either in air or in the ground as the reference. In this thesis, we chose the center point on the

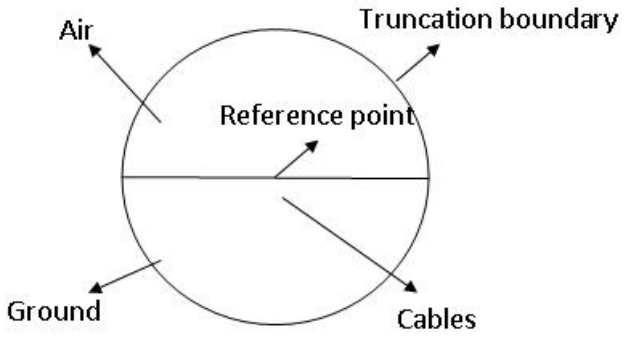

Fig. 3.2: Model used in Comsol. The bigger cirlce surrounds the cable. Upper half of this circle is air and the lower half is ground. The center of the whole circle is chosen as the reference point.

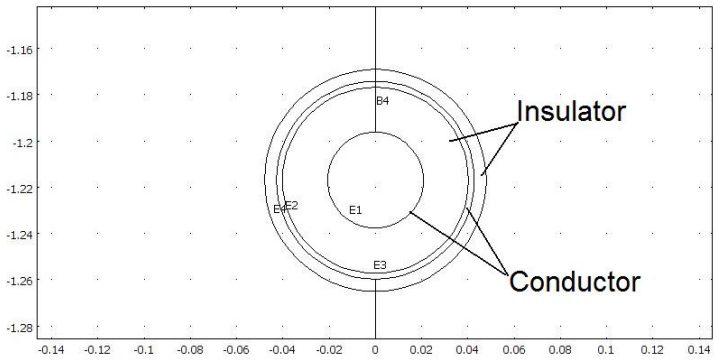

Fig. 3.3: Single cable model geometry used in full wave.

ground-air boundary right above the cables as the reference point (Fig. 3.2).

First, the propagating transmission line mode has to be found. A flow chart is given (Fig. 3.4 wo summarize the step by step process followed for the proper mode selection. For example, for a single cable system with two conductors (Fig. 3.3), there are two modes. One would be the coaxial mode (Fig. 3.5) and the other would be ground/sheath mode (Fig. 3.6). Primarily these two modes can be identified by observing the electric and magnetic field of the region. Then modes

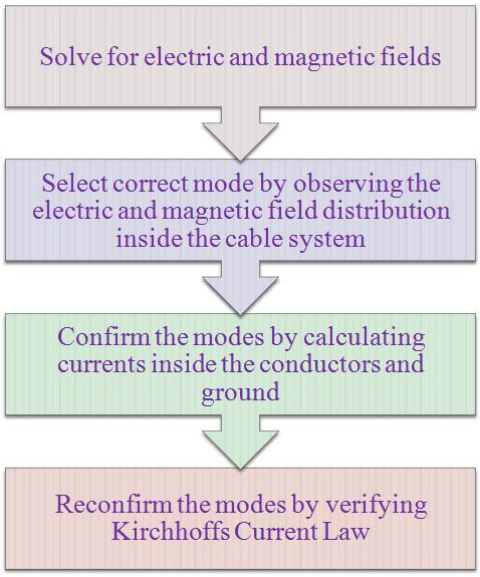

Fig. 3.4: Flow chart for selecting the proper transmission line modes.

can be confirmed by calculating the currents inside conductor, sheath and ground. For coaxial mode the current will go through the core and return through the sheath or the direction would be reverse. For ground/sheath mode the current would be only through sheath and the ground. And we can reconfirm the mode by applying KCL in the cable system which means summation of all the currents in the cable system should be zero.

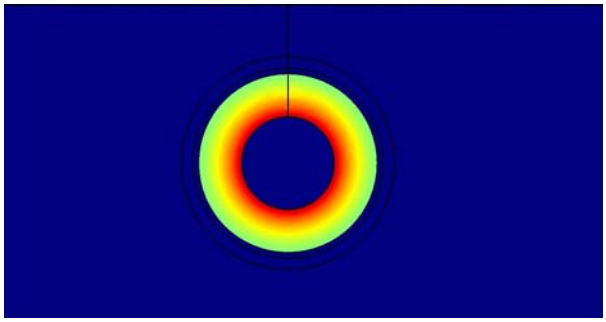

Fig. 3.5: Electric field distribution for coaxial mode of operation for a single cable

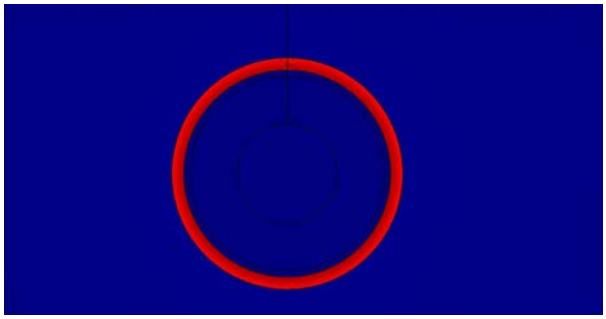

Fig. 3.6: Electric field distribution for ground/sheath mode of operation for a single cable

3.1.2 Current and Voltage Calculation

As mentioned in Section 2.2.2, the current in the conductors can be calculated by integrating the current density over the selected area using,

$$I = \int_S JdA = \int_S \sigma EdA. \tag{3.6}$$

For voltage calculation, a reference point was set. Then the voltage can be found by integrating the electric field along the line using,

$$V = -\int_h Edl. \tag{3.7}$$

3.2 PSCAD Calculation

PSCAD (Power Systems Computer Aided Design) is one of the most popular and widely used softwares for power system transient simulation. It is a time domain simulation tool to study the transient behavior of electrical networks. We choose PSCAD to analyze the same cable we analyzed using full wave method and then compare the results.

In PSCAD, modified vesion of Wedepohl's equations [1] are used for underground coaxial cable modeling. The equations are given in section 1.2. But, the limitation is, these are valid up to 1 MHz [36]. Also, PSCAD is capable of model-

ing circular shaped cables only.

PSCAD gives the per unit length $\hat{\boldsymbol{Z}}$ and $\hat{\boldsymbol{Y}}$ matrices. From here the propagation constant can be calculated. The similarity transformation matrix $\hat{\boldsymbol{T_I}}$ can be found from the eigenvector of $\boldsymbol{\hat{Y}\hat{Z}}$ and the eigenvalue of $\boldsymbol{\hat{Y}\hat{Z}}$ gives $\hat{\boldsymbol{\gamma}}^2$.

$$\begin{aligned} \hat{\boldsymbol{T_I}}^{-1}\boldsymbol{\hat{Y}\hat{Z}}\boldsymbol{T_I} &= \hat{\boldsymbol{\gamma}}^2, \\ &= \begin{bmatrix} \hat{\gamma}_1^2 & 0 & \cdots & 0 \\ 0 & \hat{\gamma}_2^2 & \ddots & \vdots \\ \vdots & \ddots & \ddots & 0 \\ 0 & \cdots & 0 & \hat{\gamma}_n^2 \end{bmatrix}. \end{aligned} \tag{3.8}$$

Phase constant $\boldsymbol{\beta}$ and attenuation constant $\boldsymbol{\alpha}$ can be calculated from propagation constant

$$\hat{\boldsymbol{\gamma}} = \boldsymbol{\alpha} + j\boldsymbol{\beta}. \tag{3.9}$$

We compared the phase constants, attenuation constants, per unit length resistances, per unit length inductances, and per unit length capacitances of the underground cables calculated using both methods.

4. CASE STUDIES

Several cases have been studied to have a clear understanding about the behavior of the transmission line model used in PSCAD and compare it with results in case of full wave simulation. We have compared the variation of phase constant (β), attenuation constant (α), per unit length (PUL) resistance (R), inductance (L) and capacitance (C) with frequency. For phase constant, we presented relative value which is calculated using,

$$\text{beta relative} = \frac{\beta_0}{\beta}, \tag{4.1}$$

where, β_0 is the propagation constant if the wave travels through vacuum and β is the calculated propagation constant.

In full wave calculation, we used operating frequencies between 500kHz and 5MHz. In lower frequencies, it becomes difficult to separate the modes of operation. Again, for lower frequencies, the truncation area for ground needs to be larger as we discussed in last chapter. It will increase the solution time. But, as we will see in our results that at lower frequencies the full wave results gradually converge with

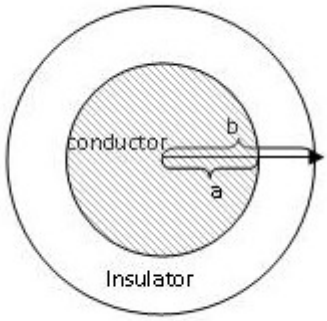

Fig. 4.1: A single conductor underground cable. Dimensions and parameters have been given in Table 4.1.

the PSCAD results. So, for lower frequencies, we can use the results from PSCAD.

4.1 A Single Cable System with One Conductor

As the first case, a simple underground cable has been studied. In this case, a cable with only core and insulator (see Fig. 4.1) has been chosen. The dimensions of the cable are given in Table 4.1.

All these parameters are chosen as default. In this chapter, we have presented a parametric study. Different cases have been studied by varying one parameter at a time.

For a single conductor cable, there is only one transmission line mode of propagation where the current goes through the conductor and comes back through

Tab. 4.1: Parameters used for a single conductor cable case

a	2 cm
b	4 cm
wire conductivity	$1 \times 10^8 S/m$
wire relative permittivity	1
wire relative permeability	1
insulator conductivity	$0 S/m$
insulator relative permittivity	3
insulator relative permeability	1
ground conductivity	$0.01 S/m$
ground relative permittivity	1
ground relative permeability	1
depth of the cable from ground surface	1 m

the ground. The electric field distribution are shown in Fig. 4.2.

4.1.1 Effect of Cable Burial Depth

First, we will analyze the effect of cable burial depth. Three different depths have been simulated.

- Cable depth 1 $=0.06m$
- Cable depth 2 $=0.14m$
- Cable depth 3 $=1m$

We have plotted the variation of the relative phase constant. As seen in Fig. 4.3, the effect is different in the case of PSCAD and full wave. In PSCAD results, the relative beta is increasing if the depth is decreased. This means the wave is slower when the depth is large. However if the cable is very near to the ground the wave is slower in the full wave analysis.

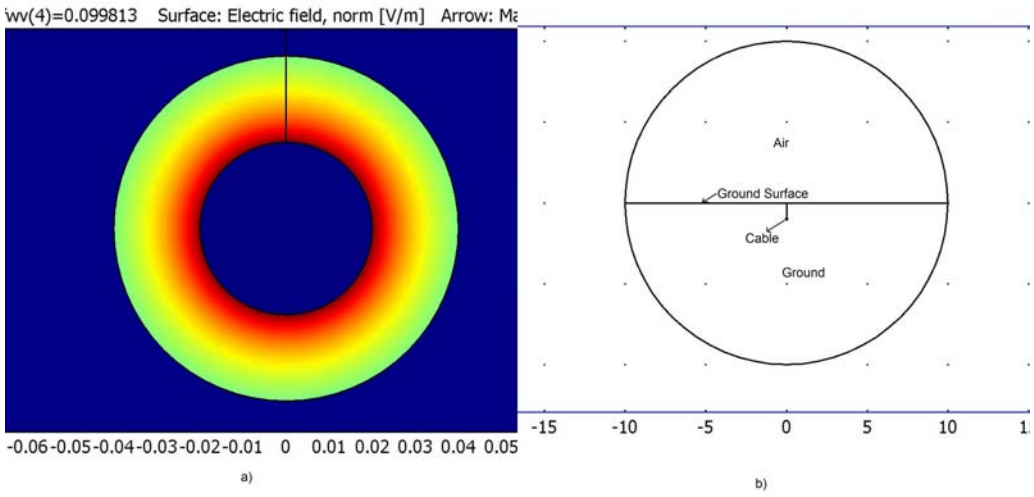

Fig. 4.2: a) Electric field distribution of a single conductor cable. b) whole model used in full wave for the single conductor cable.

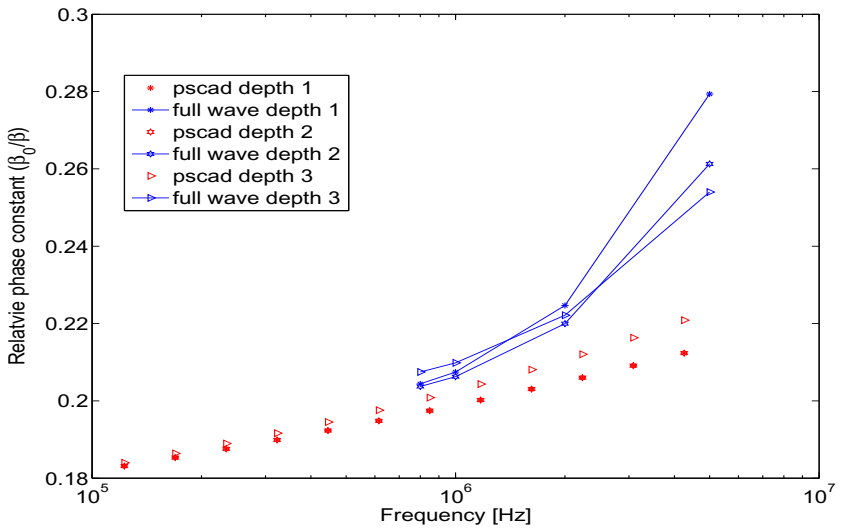

Fig. 4.3: Relative phase constant of a single conductor underground cable for three different burial depths (depth 1 = $0.06m$, depth 2 = $0.14m$. depth 3 = $1m$).

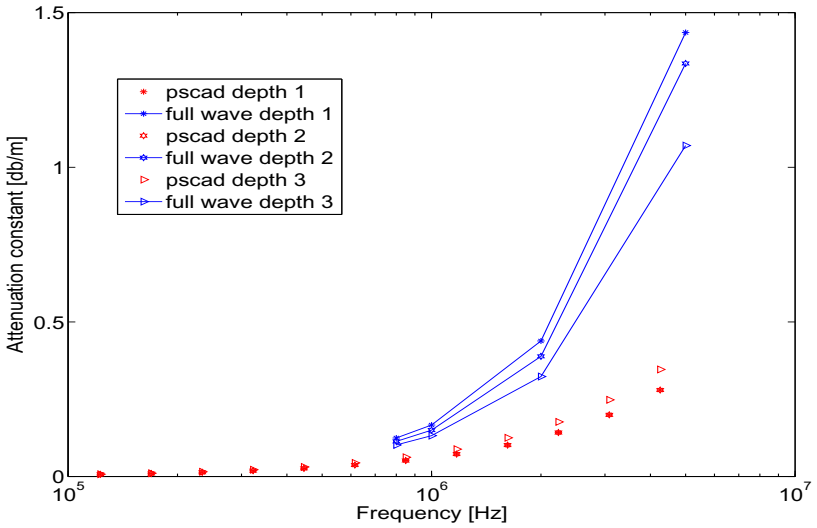

Fig. 4.4: Attenuation constant of a single conductor underground cable for three different burial depths (depth 1 = $0.06m$, depth 2 = $0.14m$. depth 3 = $1m$).

In Fig. 4.4, where we have plotted the attenuation constant, the effect of burial depth is reversed between PSCAD and full wave. If the cable depth decreases that should have similar effect of decreasing conductance of the ground, because, by decreasing the depth, we are decreasing the current flowing area at one side of the cable. So, there should be more attenuation in shallow depth. Full wave shows that effect. But, in PSCAD, the effect is reversed. Again, PSCAD cannot differentiate the effect of the small change in depth near ground surface. Full wave results are significantly different in that small change.

In Fig. 4.5 the same effect is shown by plotting the per unit length resistance. In full wave, the resistance is decreasing with the increase in cable depth. As ground resistance is included in the per unit length resistance and ground resistance

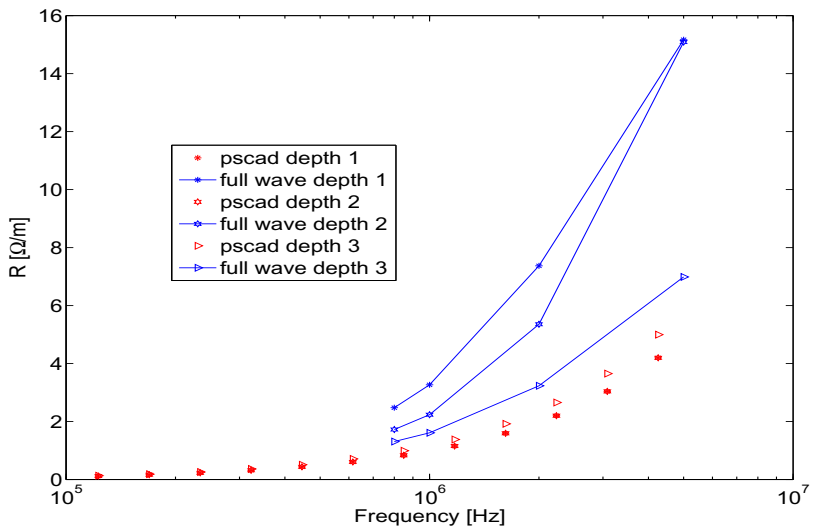

Fig. 4.5: Per unit length resistance of a single conductor underground cable for three different burial depths (depth 1 = $0.06m$, depth 2 = $0.14m$. depth 3 = $1m$).

decreases with the increase in cable depth, so the per unit length resistance should also decrease i. But PSCAD results are different. Fig. 4.6 shows the per unit length inductance values for different cable depths. The effect is quite opposite. In full wave, inductance is increasing with an increase in depth. But in PSCAD, it is decreasing.

PSCAD does not show the effect of cable depth in calculating the per unit length capacitance, but full wave method does. There is a slight variation in capacitance calculated using the full wave approach (Fig. 4.7).

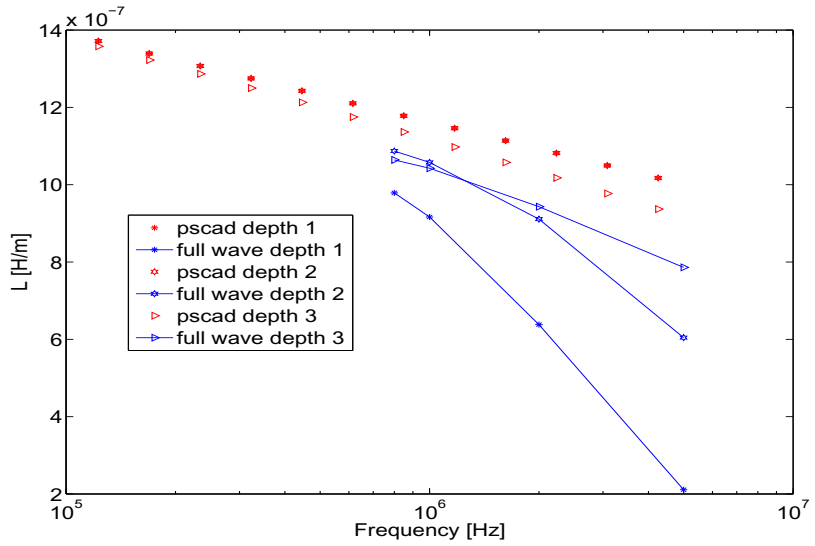

Fig. 4.6: Per unit length inductance of a single conductor underground cable for three different burial depths (depth 1 = 0.06m, depth 2 = 0.14m. depth 3 = 1m).

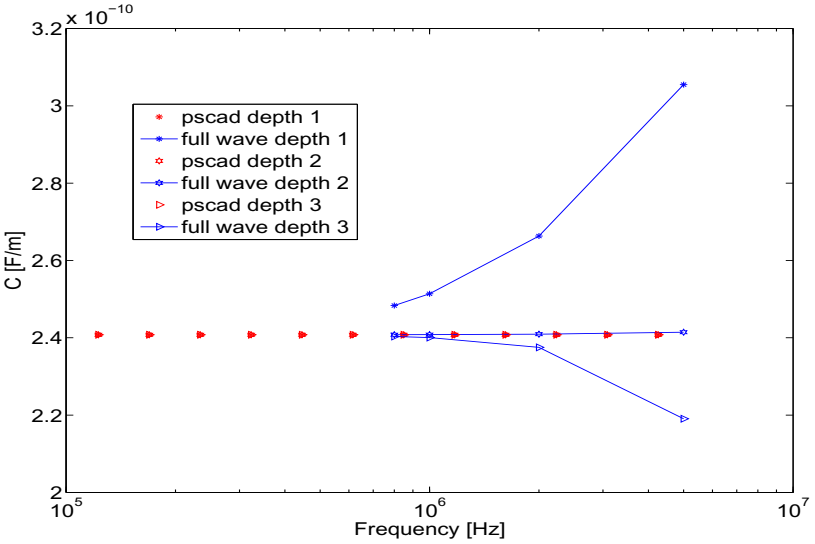

Fig. 4.7: Per unit length capacitance of a single conductor underground cable for three different burial depths (depth 1 = 0.06m, depth 2 = 0.14m. depth 3 = 1m).

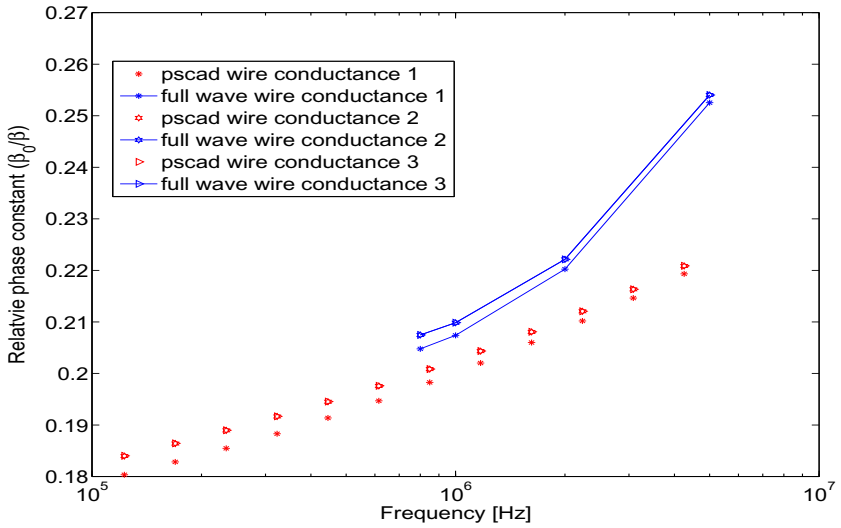

Fig. 4.8: Relative phase constant of a single conductor underground cable for three different wire conductivities (σ_1= 1×10^4 S/m, $\sigma_2 = 1\times10^8$ S/m, $\sigma_3 = 1\times10^{12}$ S/m).

4.1.2 Effect of Wire Conductivity

Conductivity of a wire can play a significant change in the the Z and Y matrix of the cable. In this section, we selected three conductivities to see its effect on the Z and Y matrices.

- Wire conductivity 1 = 1×10^4 S/m
- Wire conductivity 2 = 1×10^8 S/m
- Wire conductivity 3 = 1×10^{12} S/m

The second conductivity is close to the conductivity of typical wires used for cables. The other two is selected to test a wide range of conductivities.

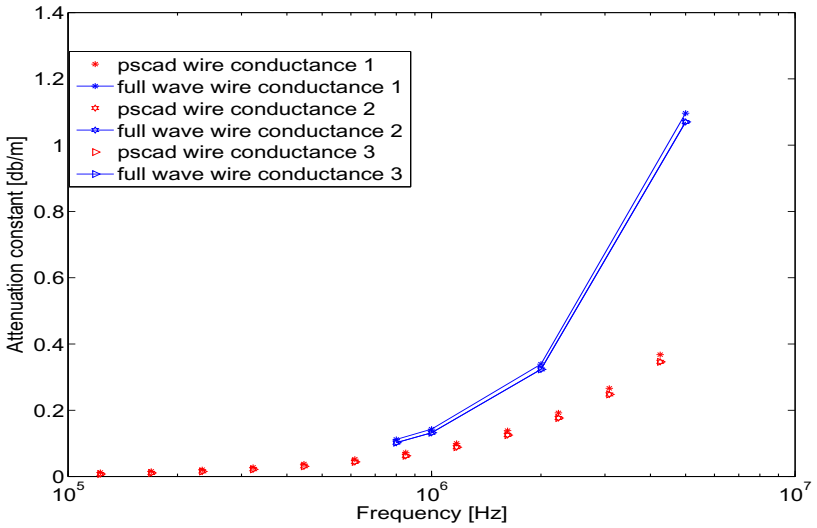

Fig. 4.9: Attenuation constant of a single conductor underground cable for three different wire conductivities ($\sigma_1 = 1 \times 10^4\ S/m$, $\sigma_2 = 1 \times 10^8\ S/m$, $\sigma_3 = 1 \times 10^{12}\ S/m$).

As shown in Figs. 4.8 and 4.9, both the propagation constant and the attenuation constant are not changing much if the conductivity is increased more than 10^8. They are almost the same. But for lower conductance, both the phase and attenuation constants are little different both in both methods. For lower conductance the attenuation is higher and the waves are slower.

For per unit length resistance (Fig 4.10) and per unit length inductance (Fig 4.11), very high wire conductivity does not have significant effect in PSCAD. In full wave, the rate of change is much higher compared to PSCAD in higher frequency region. For per unit length capacitance (Fig 4.12), PSCAD is giving only fixed values for all frequencies. But full wave method gives different values for higher

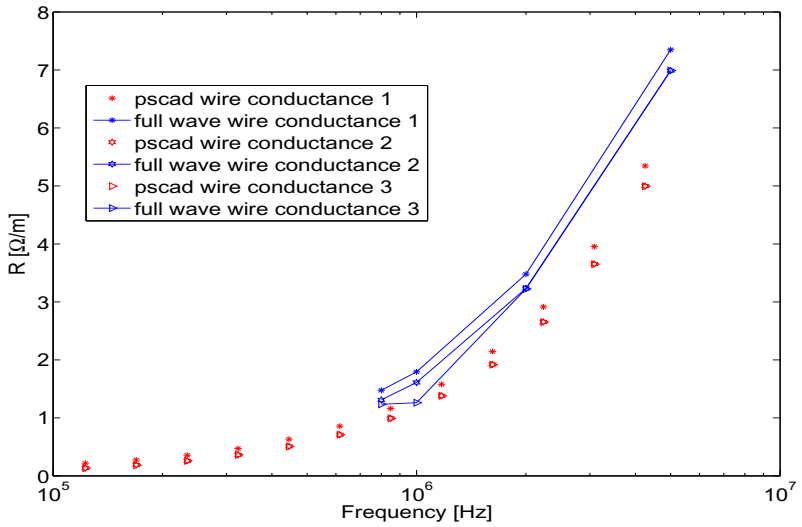

Fig. 4.10: Per unit length resistance of a single conductor underground cable for three different wire conductivities ($\sigma_1 = 1 \times 10^4\ S/m$, $\sigma_2 = 1 \times 10^8\ S/m$, $\sigma_3 = 1 \times 10^{12}\ S/m$).

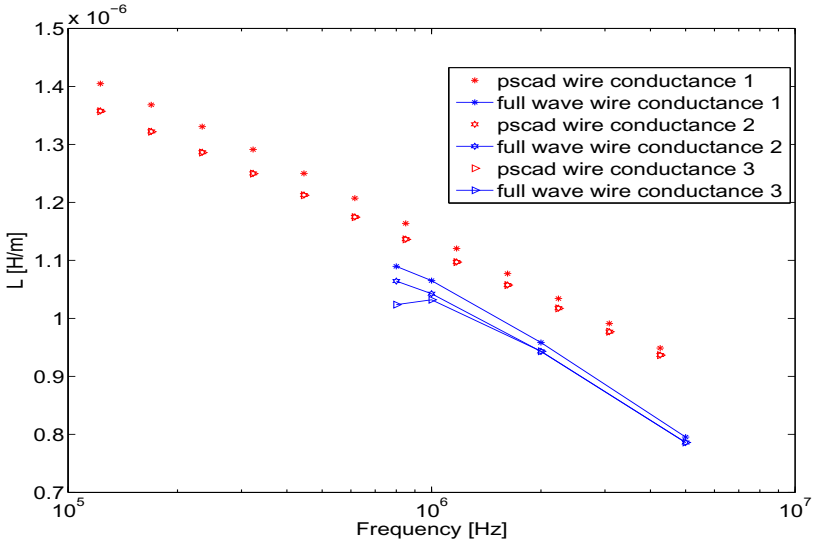

Fig. 4.11: Per unit length inductance of a single conductor underground cable for three different wire conductivities ($\sigma_1 = 1 \times 10^4\ S/m$, $\sigma_2 = 1 \times 10^8\ S/m$, $\sigma_3 = 1 \times 10^{12}\ S/m$).

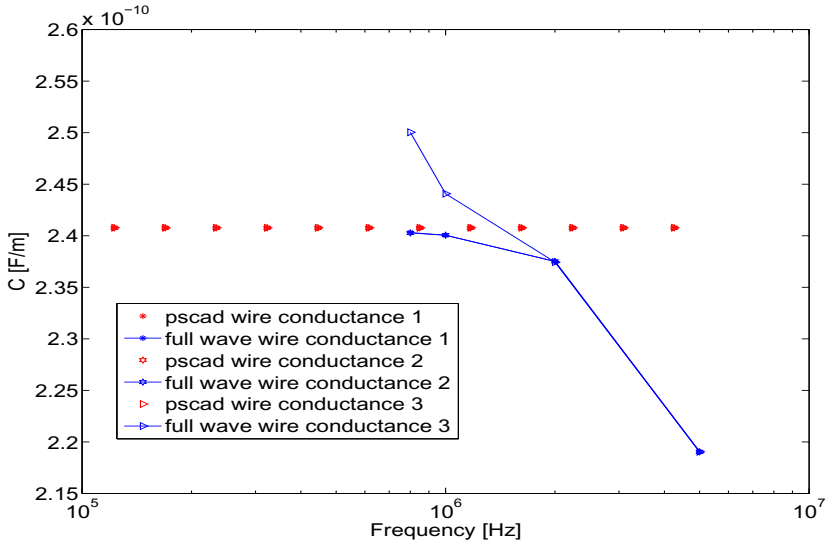

Fig. 4.12: Per unit length capacitance of a single conductor underground cable for three different wire conductivities ($\sigma_1 = 1 \times 10^4\ S/m$, $\sigma_2 = 1 \times 10^8\ S/m$, $\sigma_3 = 1 \times 10^{12}\ S/m$).

frequencies.

4.1.3 Effect of Ground Conductivity

Ground conductivity is very important for any underground cable model. It changes the circuit parameters significantly. In this section, we selected three different ground conductivities.

- Ground conductivity 1 = 0.1 S/m
- Ground conductivity 2 = 0.01 S/m
- Ground conductivity 3 = 0.002 S/m

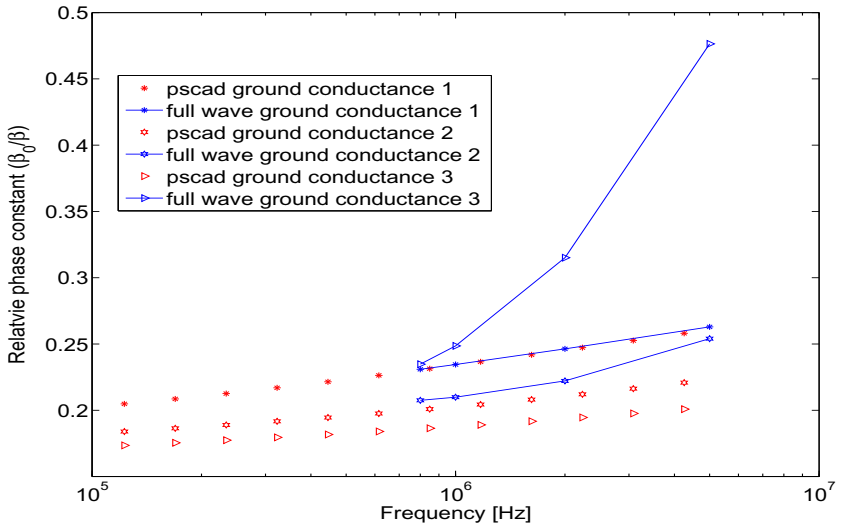

Fig. 4.13: Relative phase constant of a single conductor underground cable for three different ground conductivities ($\sigma_1 = 0.1\ S/m$, $\sigma_2 = 0.01\ S/m$, $\sigma_3 = 0.002\ S/m$).

Typical ground conductance is 0.01. So, we selected the other values to cover both more conductive (wet) and more resistive ground (dry).

As shown in Fig. 4.13, for a high ground conductance, both the PSCAD and full wave values for propagation constant are almost identical. For the ground conductance 0.01, the values are close at lower frequencies but the differences become large for higher frequencies. For very low ground conductance (0.002), propagation constants are significantly dependent on frequencies in full wave. The rate of change in values is very high at higher frequencies. But in PSCAD, the rate of change is almost same as previous two ground conductances.

According to Fig. 4.14, attenuation constant is very close in PSCAD for all

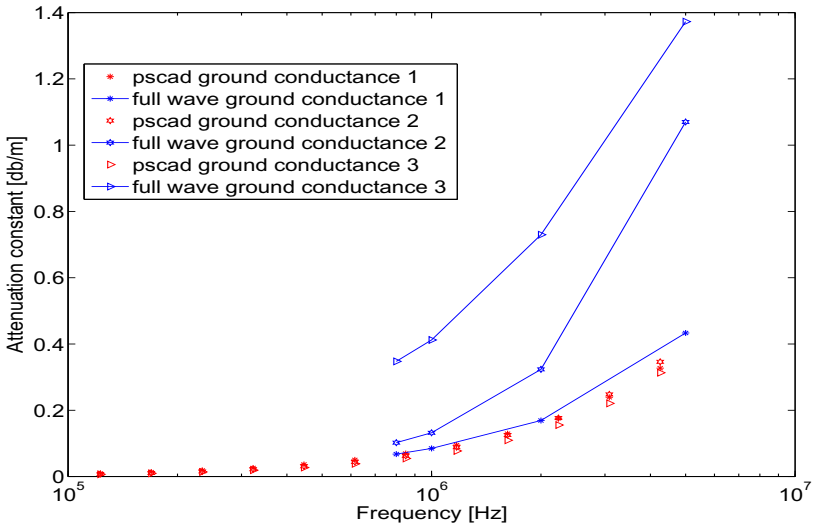

Fig. 4.14: Attenuation constant of a single conductor underground cable for three different ground conductivities ($\sigma_1 = 0.1\ S/m$, $\sigma_2 = 0.01\ S/m$, $\sigma_3 = 0.002\ S/m$).

three ground conductivities. But in full wave, attenuation is changing significantly with change in ground conductivity. If the ground conductivity is less, the attenuation is more.

By observing Fig. 4.15, 4.16, 4.17, it is clear that PSCAD and full wave values are matching closely for all frequencies only for high ground conductivities. For per unit length resistance, PSCAD values are very close for ground conductance of 0.01 and 0.002. But full wave values are significantly different.

The effect on per unit length inductance values are much more significant both in PSCAD and full wave. In PSCAD, inductance increases if the ground conductance decreases. In full wave, inductance decreases if the ground conductance

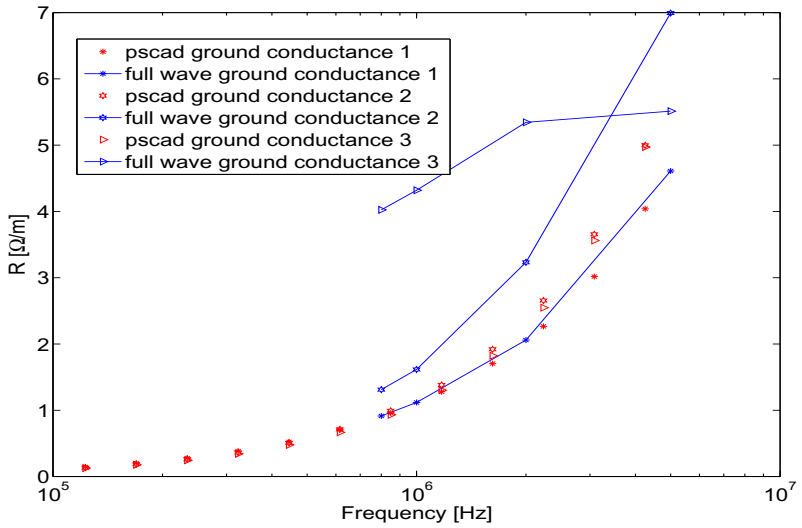

Fig. 4.15: Per unit length resistance of a single conductor underground cable for three different ground conductivities ($\sigma_1 = 0.1\ S/m$, $\sigma_2 = 0.01\ S/m$, $\sigma_3 = 0.002\ S/m$).

decreases. But the rate of change in each frequency point is similar in both methods.

PSCAD is giving a fixed per unit length capacitance value for all the ground conductances. Ground conductivity does not have any effect there. But in full wave, per unit length capacitance is changing significantly. At lower ground conductivity, the rate of change of capacitance is higher. That means, if the ground is dry (low ground conductance), the capacitance will significantly change with frequencies.

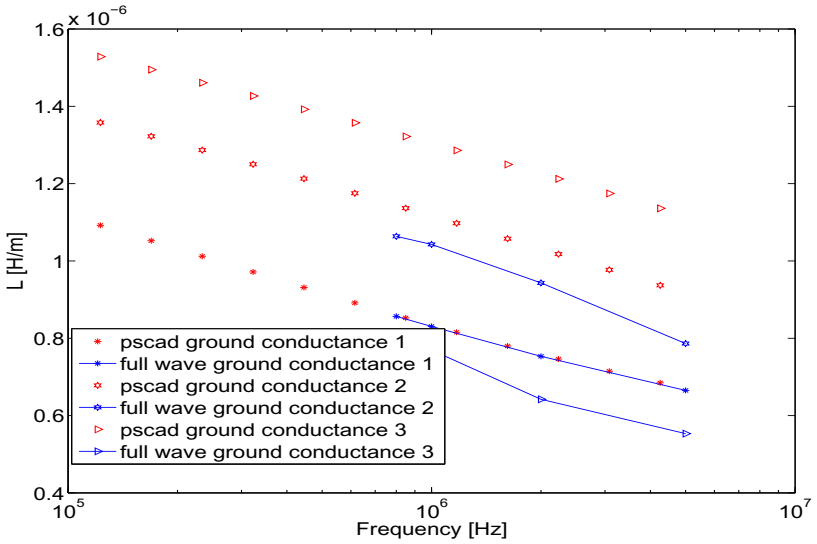

Fig. 4.16: Per unit length inductance of a single conductor underground cable for three different ground conductivities ($\sigma_1 = 0.1\ S/m$, $\sigma_2 = 0.01\ S/m$, $\sigma_3 = 0.002\ S/m$).

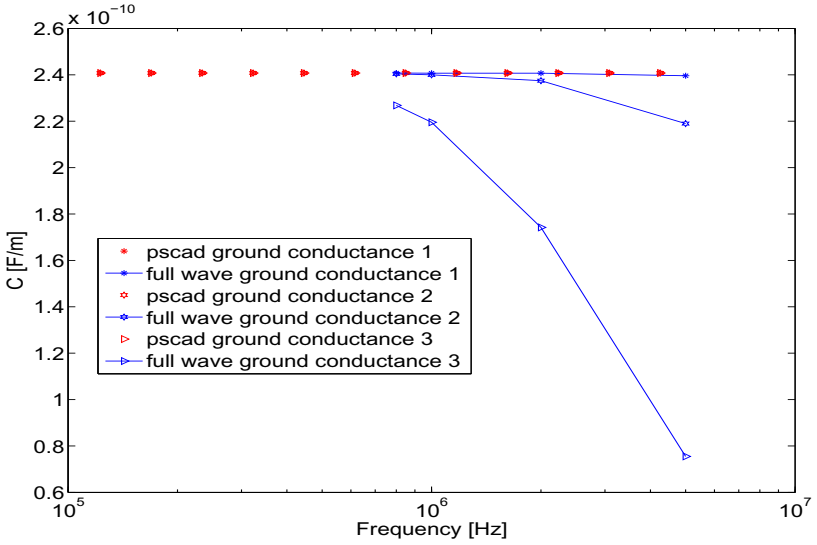

Fig. 4.17: Per unit length capacitance of a single conductor underground cable for three different ground conductivities ($\sigma_1 = 0.1\ S/m$, $\sigma_2 = 0.01\ S/m$, $\sigma_3 = 0.002\ S/m$).

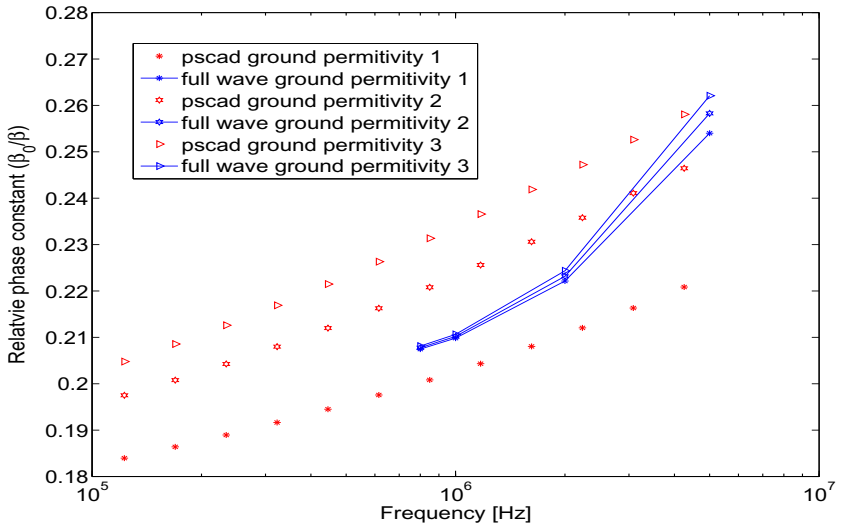

Fig. 4.18: Relative phase constant of a single conductor underground cable for three different relative permitivitties of ground (ϵ_{r1}= 1, ϵ_{r2} = 5, ϵ_{r3} = 10).

4.1.4 Effect of Ground Permittivity

Three different ground permittivities are selected for this study.

- Ground relative permittivity 1 = 1
- Ground relative permittivity 2 = 5
- Ground relative permittivity 3 = 10

Ground permittivity (Fig. 4.18) does not have significant effect on propagation constant when full wave method was used. But the change is more significant in PSCAD. In both methods, propagation constant decreases when the permittivity increases.

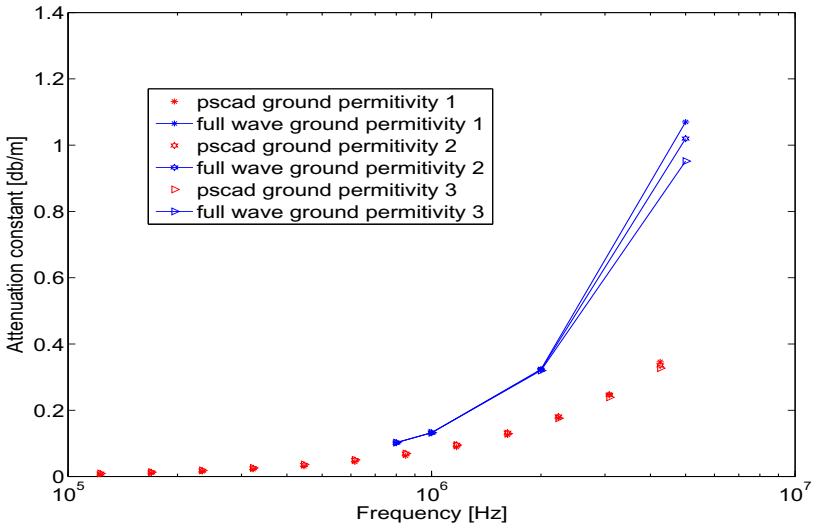

Fig. 4.19: Attenuation constant of a single conductor underground cable for three different relative permittivities of ground (ϵ_{r1}= 1, ϵ_{r2} = 5, ϵ_{r3} = 10).

The effect is less in both methods for attenuation constant (Fig. 4.19). In PSCAD, the values are very close. In full wave, the effect is more prominent for higher frequencies. At higher frequency region, difference between the results from two method become significant. The per unit length resistance is affected by the ground permittivity only at higher frequencies in both method. In PSCAD, the difference is larger.

In full wave, per unit length inductance (Fig. 4.21) is not affected by ground permittivity. But in PSCAD the effect is very significant.

PSCAD fails to show the change in the per unit length capacitance (Fig. 4.21) when the ground permittiviy changes. But in full wave the effect is clear. And the difference becomes more in higher frequencies. Theoretically ground permittivity

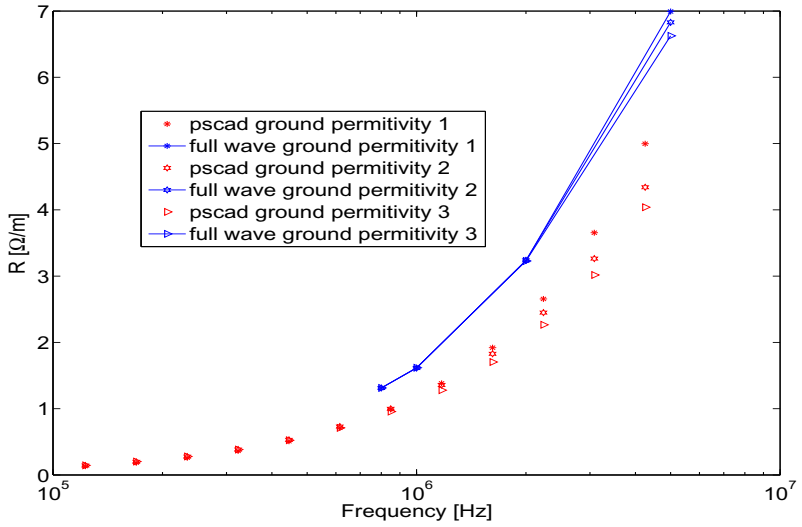

Fig. 4.20: Per unit length resistance of a single conductor underground cable for three different relative permittivities of ground (ϵ_{r1}= 1, ϵ_{r2} = 5, ϵ_{r3} = 10).

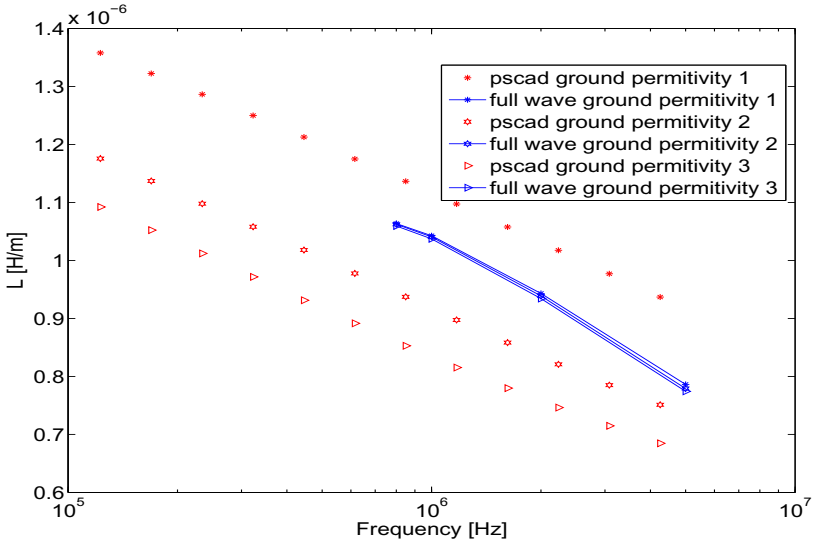

Fig. 4.21: Per unit length inductance of a single conductor underground cable for three different relative permittivities of ground (ϵ_{r1}= 1, ϵ_{r2} = 5, ϵ_{r3} = 10).

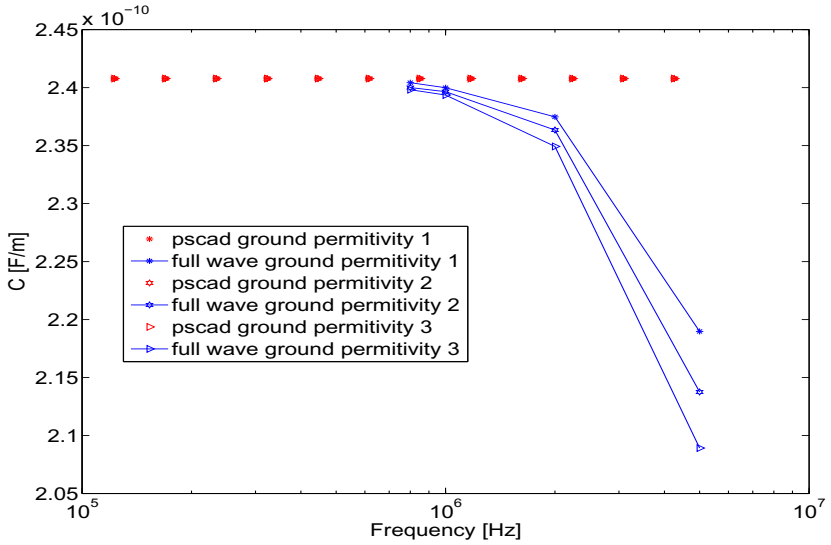

Fig. 4.22: Per unit length capacitance of a single conductor underground cable for three different relative permittivities of ground (ϵ_{r1}= 1, ϵ_{r2} = 5, ϵ_{r3} = 10).

should have significant effect in calculation of capacitance. PSCAD fails to model that. On the other hand, inductance should not change much with change in ground permittivity. PSCAD models gives a significant change in inductance. In both cases,full wave method gives results which can be explained by theory.

4.2 A Single Cable System with Two Conductors

In this section, we will analyze a underground cable system with two conductors. The cable has both core and sheath. The dimensions of the cable are shown in Fig. 4.23 and the parameters are given in Table 4.2:

The values, given here, are the default parameters. One parameter has been changed at a time to analyze the effect.

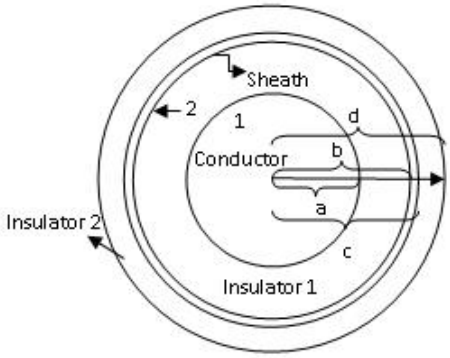

Fig. 4.23: A single cable with a conductor (or core) and a sheath. The core and the sheath are numbered as conductor 1 and 2. Values for radius a, b, c and d are given in Table 4.2.

Tab. 4.2: Parameters used for a single cable with a core and a sheath case

a	2 cm
b	4 cm
c	4.25 cm
d	5 cm
core conductivity	$1 \times 10^8 S/m$
sheath conductivity	$1 \times 10^8 S/m$
core and sheath relative permittivity	1
core and sheath relative permeability	1
insulator 1 and 2 conductivity	0
insulator 1 relative permittivity	3
insulator 2 relative permittivity	2
insulator 1 and 2 relative permeability	1
ground conductivity	$0.01 S/m$
ground relative permittivity	1
ground relative permeability	1
depth of the cable from ground surface	1 m

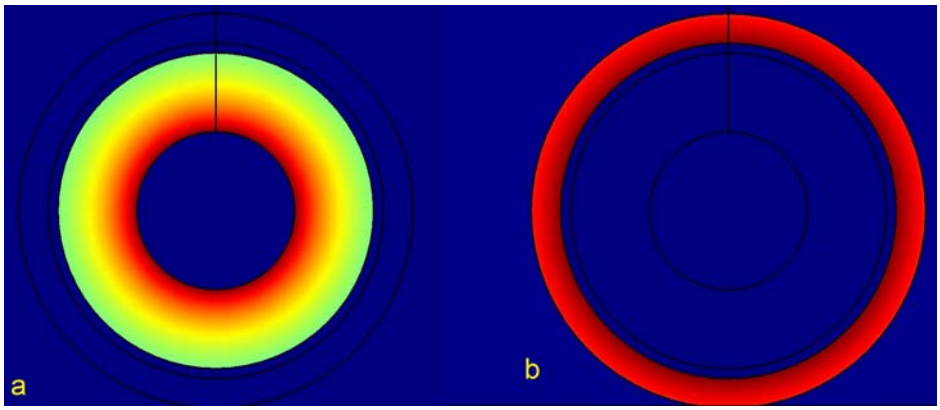

Fig. 4.24: Electric field distribution for two modes of operation of a single cable system with a conductor and a sheath: a) coaxial mode of operation, b) ground mode of operation.

For this cable, there are two modes of operation (Figure 4.24): coaxial and ground. In coaxial mode, current goes through the core and comes back through the sheath or vice versa. In ground mode (it is also called sheath mode), current goes through the sheath and comes back through the ground or vice versa. In full wave, we can separate the modes during simulation. But, in case of PSCAD calculation, the calculation of propagation constant is done in a set of frequencies. And during this process mode switching happens quiet few times. So, it is difficult to separate all the modes. To overcome this problem, we plot all the modes in the same figure which gives us a complete idea of all the modes.

4.2.1 Effect of Cable Depth

At first we will analyze the effect of cable burial depth. Three depths were chosen as follow,

- Cable depth 1 = $0.06m$
- Cable depth 2 = $0.15m$
- Cable depth 3 = $1m$

As shown in Fig. 4.25, for coaxial mode, the propagation constant for both PSCAD and full wave method is matching almost exactly. For ground mode, we are getting same kind of results as found in the single conductor cable inside the ground (Fig. 4.3). PSCAD values are very close to each other. Full wave method gives slightly different phase constants at higher frequencies. Another important point is that, in full wave method, beta increases if the cable depth is decreased, which means that wave in the sheath mode travels faster if the cable depth is increased.

Attenuation constants (Fig. 4.26) for coaxial mode is almost the same in both methods. But in ground mode, they are different.

The effect of cable depth on per unit length resistance (Fig. 4.27) is more significant in full wave method. R11, R12 and R13 are decreasing with increase in the cable depth. But the effect is opposite in PSCAD. Theoretically when the depth is very small, then the ground current has a small area to flow. So, the

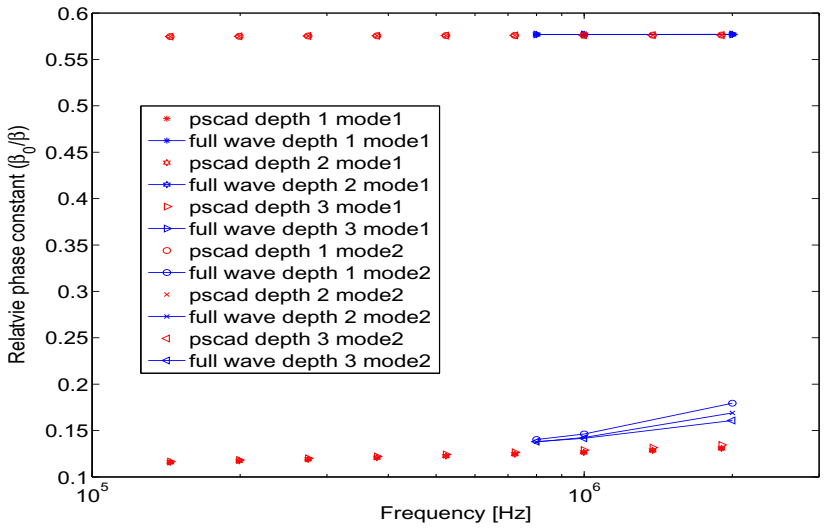

Fig. 4.25: Relative phase constant of a single underground cable for three different burial depths (depth 1 = $0.06m$, depth 2 = $0.15m$, depth 3 = $1m$.

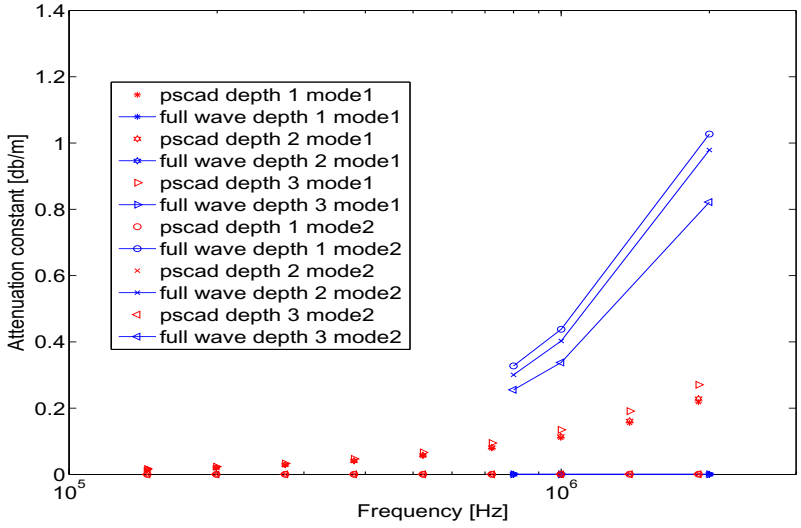

Fig. 4.26: Attenuation constant of a single underground cable for three different burial depths (depth 1 = $0.06m$, depth 2 = $0.15m$, depth 3 = $1m$).

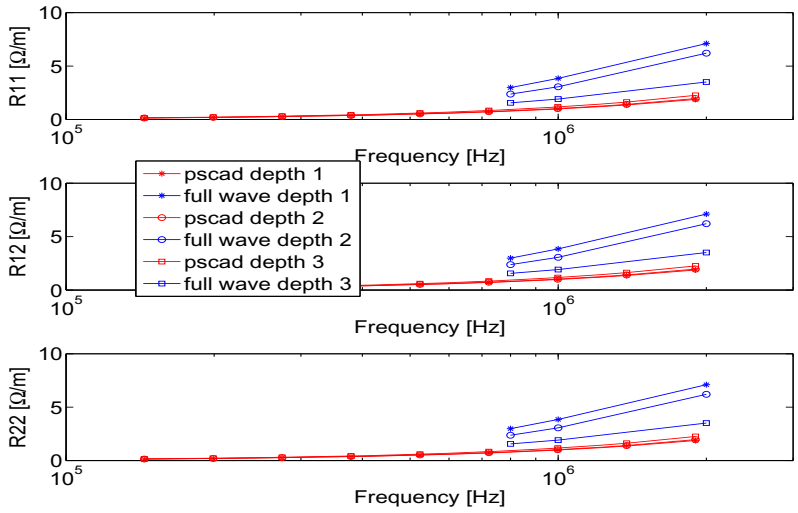

Fig. 4.27: Per unit length resistance of a single underground cable for three different burial depths (depth 1 = $0.06m$, depth 2 = $0.15m$, depth 3 = $1m$).

effective ground resistance should decrease for larger depth. Full wave results are consistent with this observation.

Both the per unit length self inductance and mutual inductance (Fig. 4.28) decrease significantly when the cable is buried deeper in the ground. But in PSCAD the change is not that significant. Moreover, the change in PSCAD is in reverse direction when compared to full wave method.

The per unit length self capacitance of the core and the mutual capacitance (Fig. 4.29) is almost fixed in both methods. C11 and C12 are almost same in both methods. But the self capacitance of sheath changes in the full wave method.

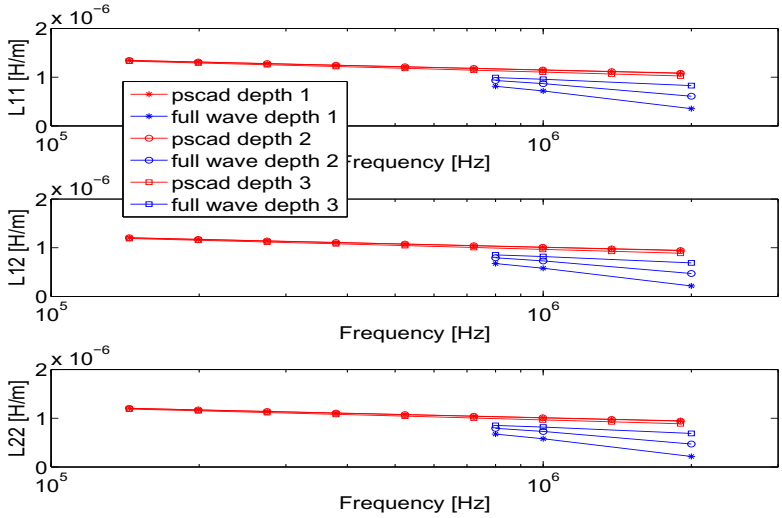

Fig. 4.28: Per unit length inductance of a single underground cable for three different burial depths (depth 1 = 0.06m, depth 2 = 0.15m, depth 3 = 1m).

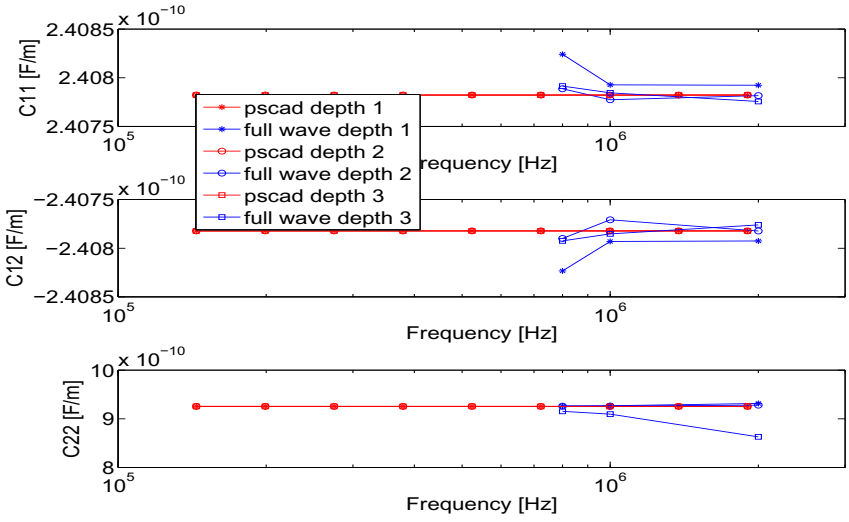

Fig. 4.29: Per unit length capacitance of a single underground cable for three different burial depths (depth 1 = 0.06m, depth 2 = 0.15m, depth 3 = 1m).

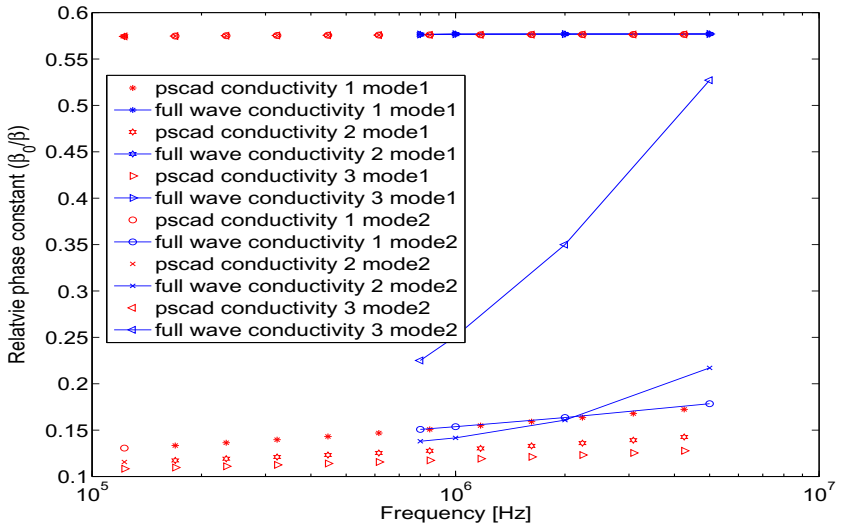

Fig. 4.30: Relative phase constant of a single underground cable for three different ground conductivities ($\sigma_1 = 0.1\ S/m$, $\sigma_2 = 0.01\ S/m$, $\sigma_3 = 0.002\ S/m$).

4.2.2 Effect of Ground Conductivity

Similar to the single conductor cable case, we selected three ground conductivities for analysis. They are:

- Ground conductivity 1 = 0.1 S/m
- Ground conductivity 2 = 0.01 S/m
- Ground conductivity 3 = 0.002 S/m

As shown in Figs. 4.30 and 4.31, we can see that both the propagation and attenuation constants are almost same in both PSCAD and full wave for the coaxial mode but different for the ground mode. When the ground conductivity is high then beta is matching as well for both methods. But for lower ground conductivity

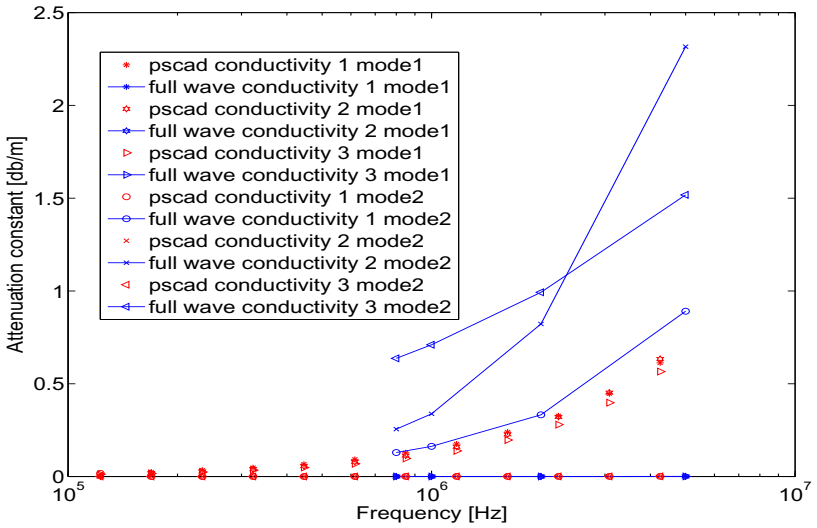

Fig. 4.31: Attenuation constant of a single underground cable for three different ground conductivities ($\sigma_1 = 0.1\ S/m$, $\sigma_2 = 0.01\ S/m$, $\sigma_3 = 0.002\ S/m$).

β is different in two methods. The rate of change of beta with respect to frequency is increasing with a decrease in ground conductivity.

Th per unit length resistance (Fig. 4.32), inductance (Fig. 4.33) and capacitance (Fig. 4.34) are matching when the ground conductivity is high but different for other conductivities. In PSCAD, capacitance is fixed as previous. But in full wave, C22 varies with frequencies. C11 and C12 have almost same values in both methods.

4.2.3 Effect of Ground permittivity

We used the same set of permittivities as used in the single cable system with single conductor case. They are:

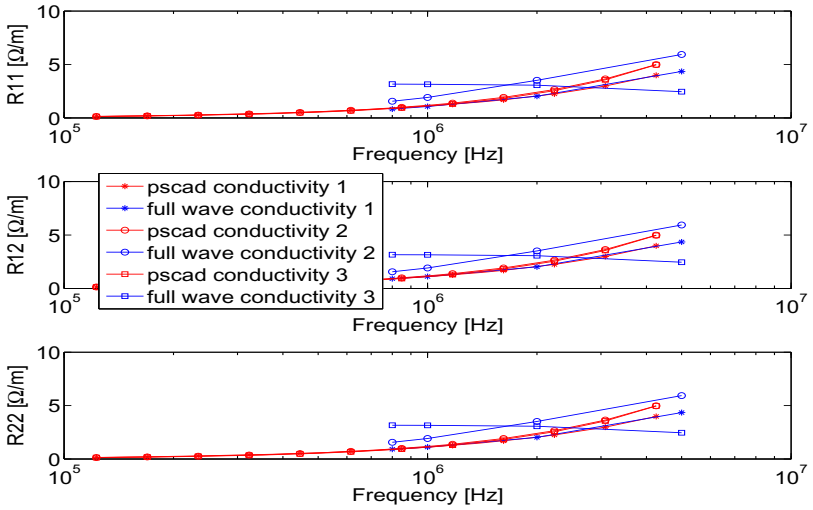

Fig. 4.32: Per unit length resistance of a single underground cable for three different ground conductivities ($\sigma_1 = 0.1\ S/m$, $\sigma_2 = 0.01\ S/m$, $\sigma_3 = 0.002\ S/m$).

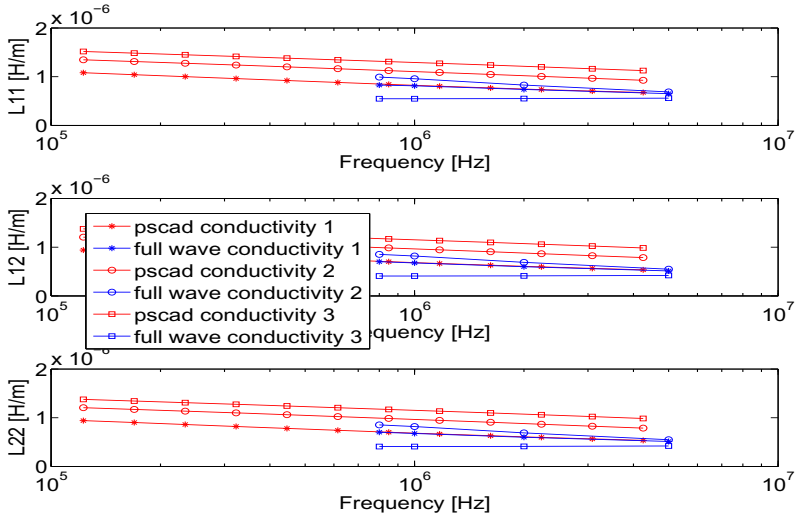

Fig. 4.33: Per unit length inductance of a single underground cable for three different ground conductivities ($\sigma_1 = 0.1\ S/m$, $\sigma_2 = 0.01\ S/m$, $\sigma_3 = 0.002\ S/m$).

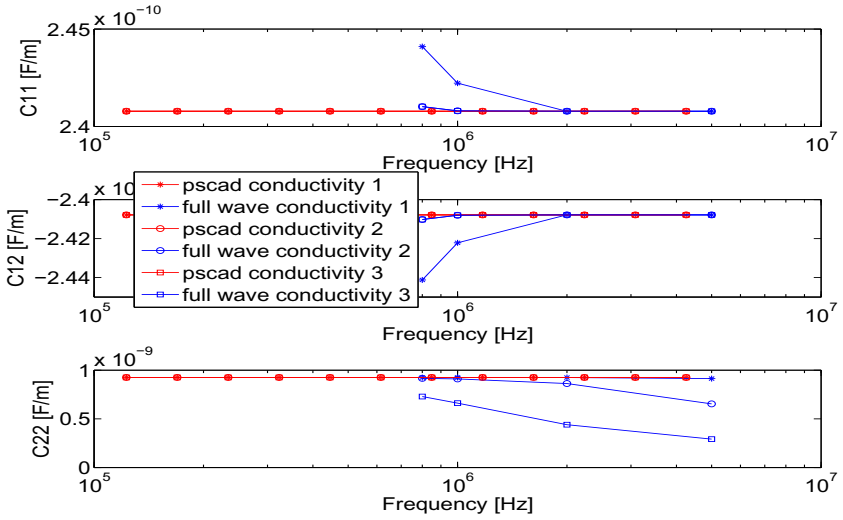

Fig. 4.34: Per unit length capacitance of a single underground cable for three different ground conductivities ($\sigma_1 = 0.1\ S/m$, $\sigma_2 = 0.01\ S/m$, $\sigma_3 = 0.002\ S/m$).

- Ground relative permittivity 1 = 1
- Ground relative permittivity 2 = 5
- Ground relative permittivity 3 = 10

The results are similar to the single conductor case.

Ground permittivity does not have much effect on both propagation (Fig. 4.35) and attenuation constants (Fig. 4.36). In PSCAD, β is considerably effected. In full wave method, α is considerably effected.

Significant differences are observed in case of the per unit length inductance (Fig. 4.38) and capacitance (Fig. 4.39). In PSCAD, inductance is effected by the different ground permittivity while capacitance is fixed. In full wave, inductance is not effected by ground permittivity but the self capacitance of the sheath (C22)

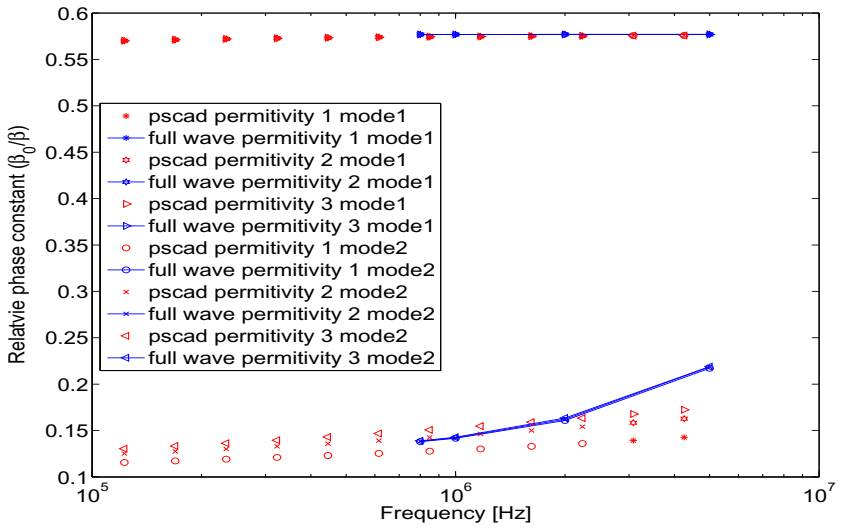

Fig. 4.35: Relative phase constant of a single underground cable for three different relative permittivities of ground ($\epsilon_{r1} = 1$, $\epsilon_{r2} = 5$, $\epsilon_{r3} = 10$).

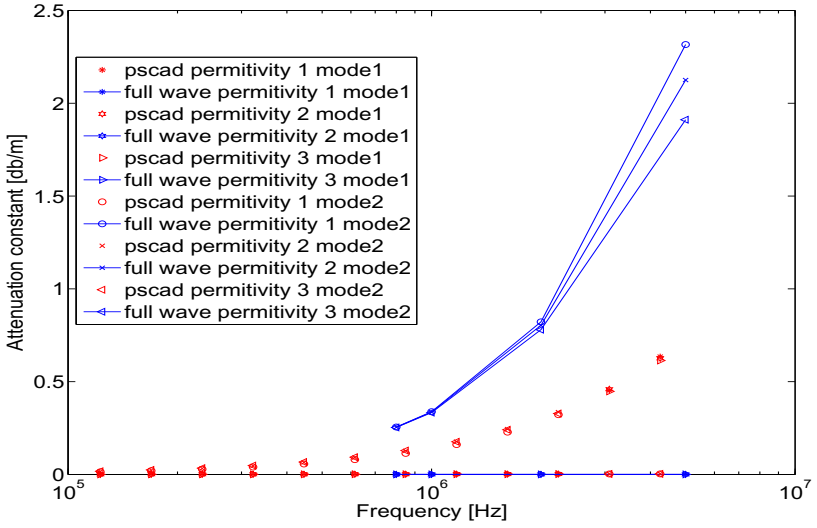

Fig. 4.36: Attenuation constant of a single underground cable for three different relative permittivities of ground ($\epsilon_{r1} = 1$, $\epsilon_{r2} = 5$, $\epsilon_{r3} = 10$).

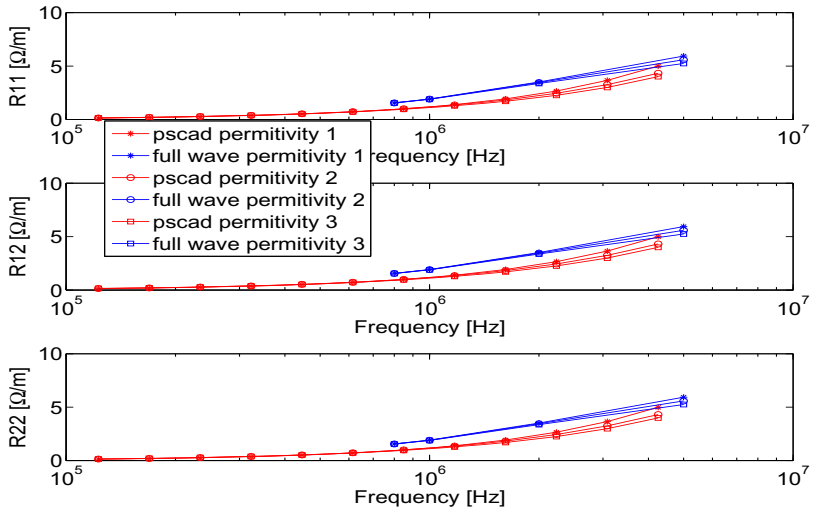

Fig. 4.37: Per unit length resistance of a single underground cable for three different relative permittivities of ground ($\epsilon_{r1} = 1$, $\epsilon_{r2} = 5$, $\epsilon_{r3} = 10$).

is significantly effected. We got the same kind of result in the single conductor cable case and discussed that the result in full wave method can be explained by theory.

4.3 A Two Cable System with Four Conductors

In this section, we will analyze two cables (Fig. 4.40). Each cable has both core and sheath. The dimensions of each cable are same as given in Table 4.2 The default distance between the two cables is 0.1m which means they are touching each other. We will change this distance between cables to analyze the effect.

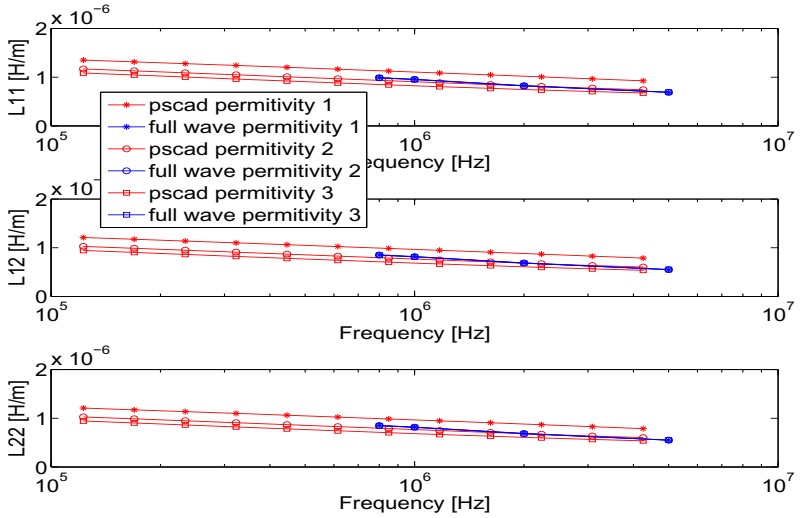

Fig. 4.38: Per unit length inductance of a single underground cable for three different relative permittivities of ground ($\epsilon_{r1} = 1$, $\epsilon_{r2} = 5$, $\epsilon_{r3} = 10$).

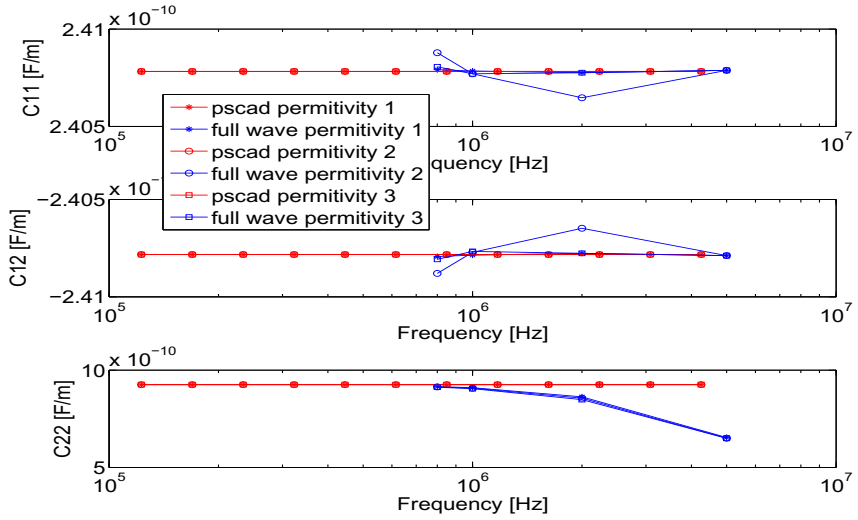

Fig. 4.39: Per unit length capacitance of a single underground cable for three different relative permittivities of ground ($\epsilon_{r1} = 1$, $\epsilon_{r2} = 5$, $\epsilon_{r3} = 10$).

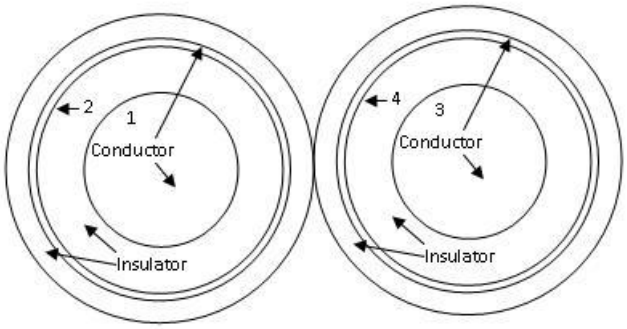

Fig. 4.40: Two cable system. There are four conductors. Each conductors are numbered as in the figure.

4.3.1 Effect of Distance Between Cables

Three distance are chosen as follow:

- Cable distance 1 =$0.1m$(touching with each other)
- Cable distance 2 =$0.2m$
- Cable distance 3 =$1.1m$

In PSCAD method, we can see the switching of the modes clearly in Fig. 4.42 . Another problem arises with this method. Some of the phase constants (β) become negative which cannot be explained. In two cable line, there are four modes. Two of them are coaxial, one is intersheath and the other is ground mode. In intersheath mode, the current flows through one sheath and comes back through the other sheath. In ground mode the current flows through both of the sheaths and comes back through ground.

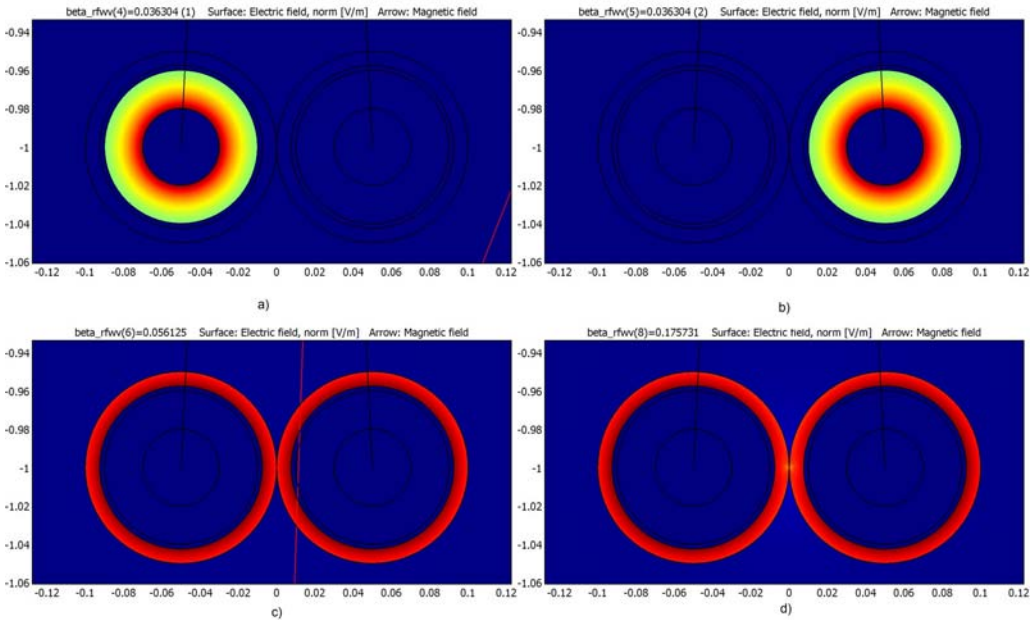

Fig. 4.41: Electric field distributions for four modes of operation of two cable. Four modes are: a) coaxial mode 1, b) coaxial mode 2, c) inter sheath mode, d) ground mode.

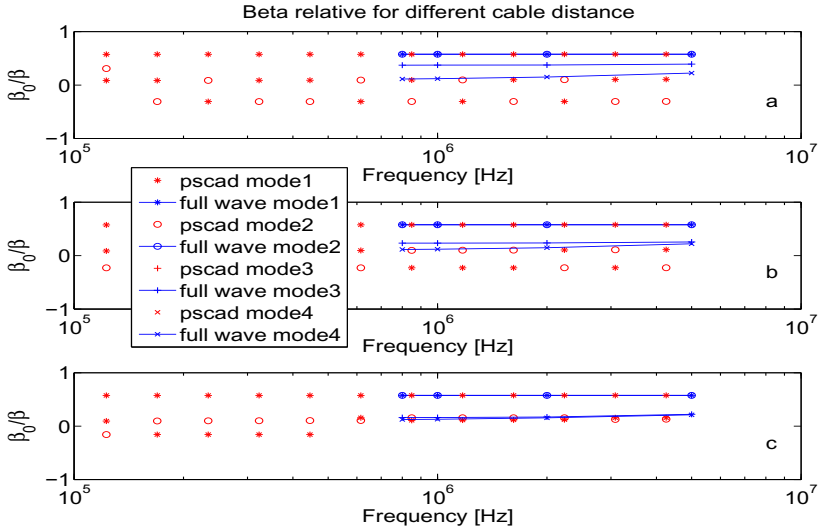

Fig. 4.42: Relative phase constant of the two cable system for different cable distances (dist. 1 =0.1m, dist. 2 =0.2m, dist. 3 =1.1m). Here a, b, and c are figures for cable distance 1, 2, and 3.

Both the propagation and attenuation constants are same in both method for coaxial modes. When cables are touching, the β for inter sheath and ground modes are different in both method. And from Fig. 4.42, we can see that the wave travels fastest in both coaxial modes. And they are not affected by change in frequencies. Wave travels faster in sheath mode than in ground mode. When cables are too far away, the act like two single cable in ground. So, the intersheath and ground mode become very close.

According to Fig. 4.44, PSCAD does not show any change in resistance when we vary the distances. But full wave values changes lightly with the change in distance.

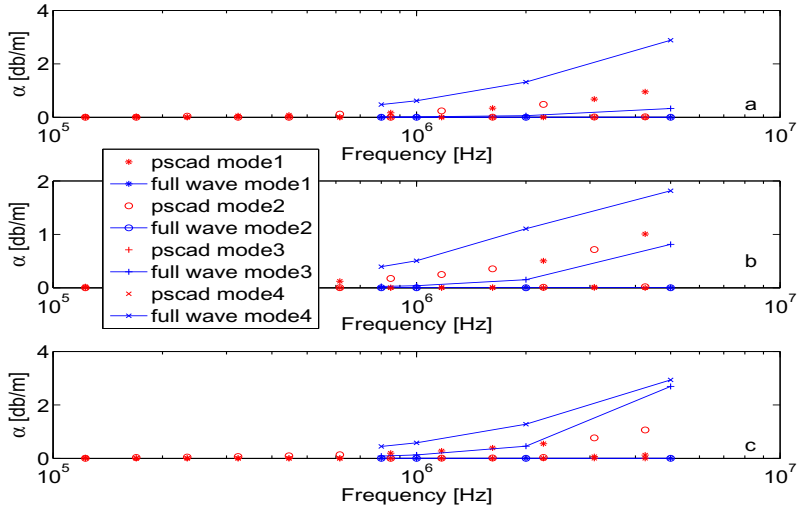

Fig. 4.43: Attenuation constant of the two cable system for different cable distances (dist. 1 =0.1m, dist. 2 =0.2m, dist. 3 =1.1m). Here a, b, and c are figures for cable distance 1, 2, and 3.

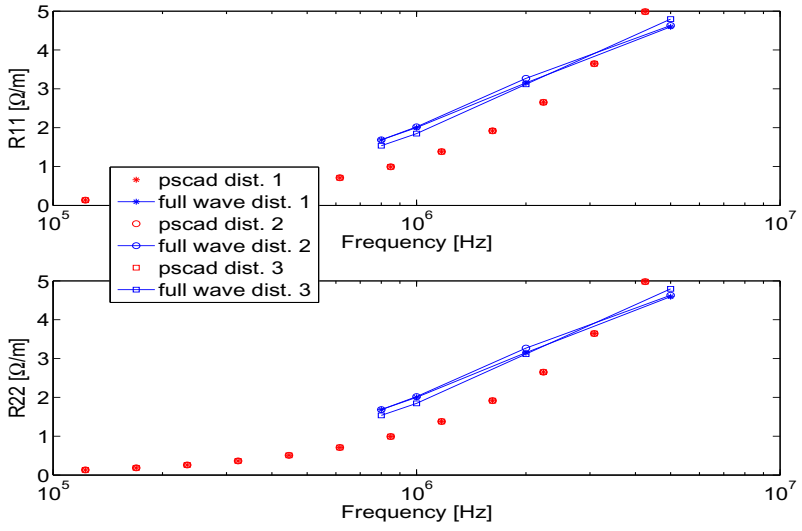

Fig. 4.44: Diagonal elements of per unit length resistance matrix of the two cable system for different cable distances (dist. 1 =0.1m, dist. 2 =0.2m, dist. 3 =1.1m).

s

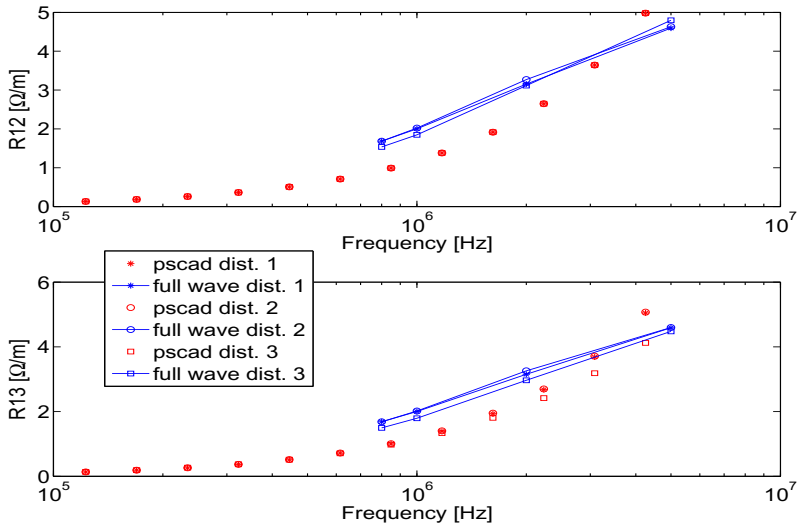

Fig. 4.45: Off diagonal elements of per unit length resistance matrix of the two cable system for different cable distances (dist. 1 =0.1m, dist. 2 =0.2m, dist. 3 =1.1m).

In Fig. 4.46, we can see that the per unit length self inductance is not changing much in PSCAD. But in full wave method, the values are quite different for three distances.

PSCAD gives fixed per unit length capacitance (Fig. 4.47) for all the cases and for all the frequencies. But in full wave, C22 changes with frequencies. Moreover, C22 varies if the cable distance is varied. C13 is very small in full wave. It should be considered as zero. C11 and C12 have almost same value in both method for all frequencies.

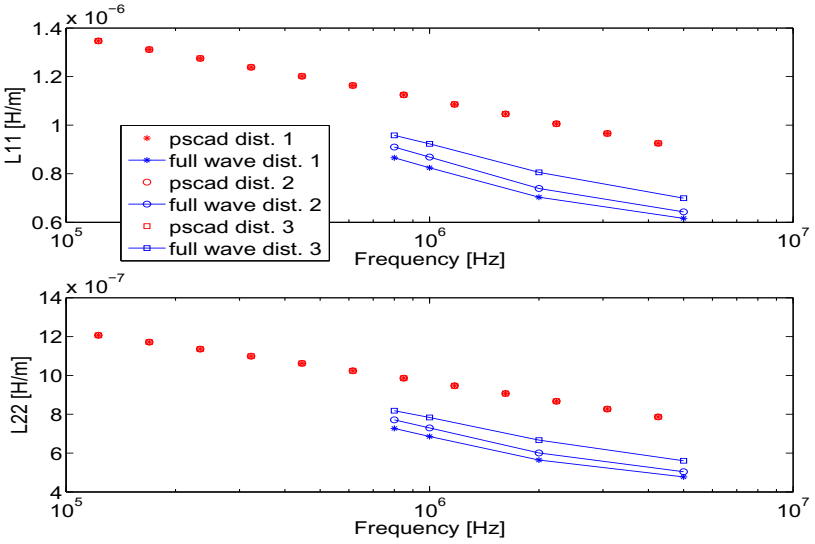

Fig. 4.46: Per unit length self inductance of the two cable system for different cable distances (dist. 1 =0.1m, dist. 2 =0.2m, dist. 3 =1.1m).

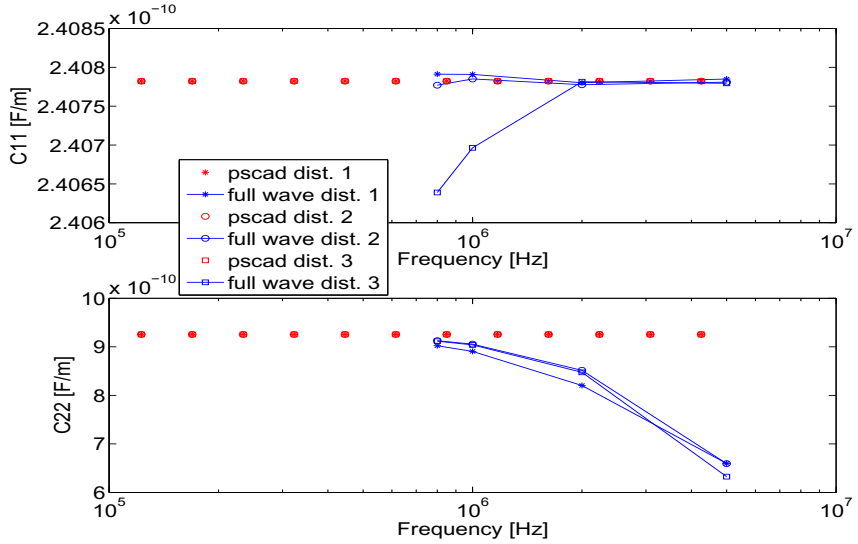

Fig. 4.47: Per unit length self capacitance of the two cable system for different cable distances (dist. 1 =0.1m, dist. 2 =0.2m, dist. 3 =1.1m).

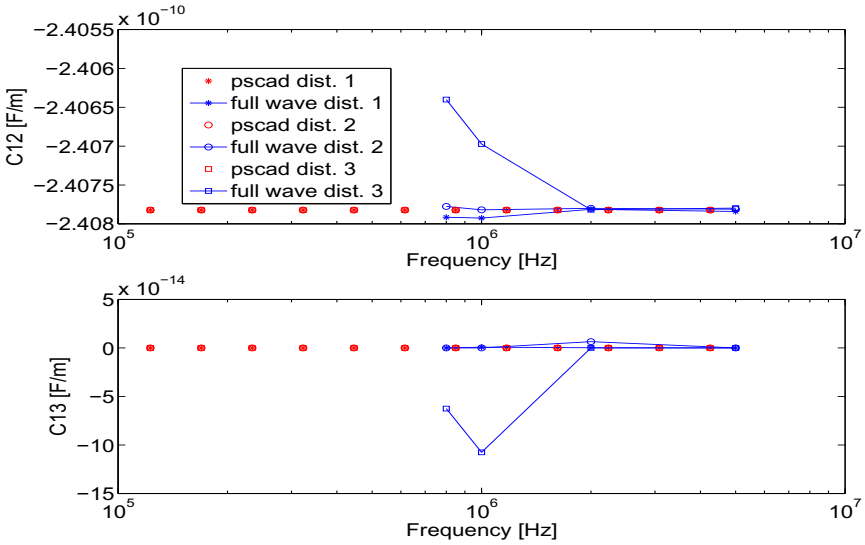

Fig. 4.48: Per unit length mutual capacitance of the two cable system for different cable distances (dist. 1 =0.1m, dist. 2 =0.2m, dist. 3 =1.1m).

4.4 A Three Cable System with Six Conductors

In this section, we will analyze a three cable system (Fig. 4.49). Each cable has both core and sheath. The dimensions of each cable are described in Table 4.2. All cables are touching to each other. The depth of the cable (distance between center of the lowest cable and the surface) is 1m .

In this case, there are six modes of operation (Fig. 4.50). Three of them are coaxial modes for three cables. Two of them are intersheath mode which means the current flows through one sheath and returns through other sheaths. The last one is ground mode, where the current flows through all the sheath and returns through the ground.

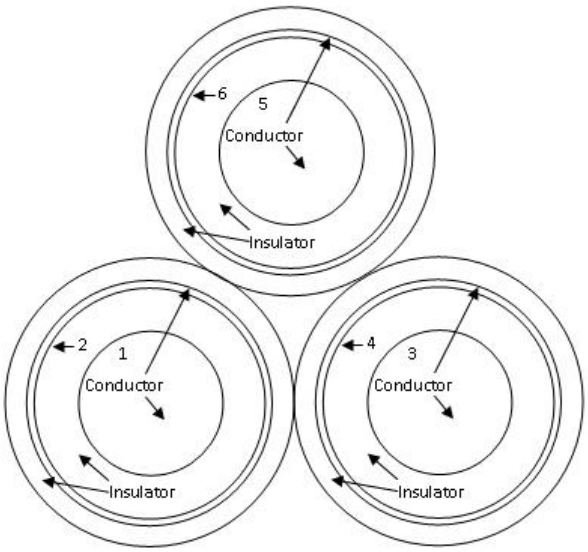

Fig. 4.49: A three cable system. There are six conductors. Each conductors are numbered as in the figure.

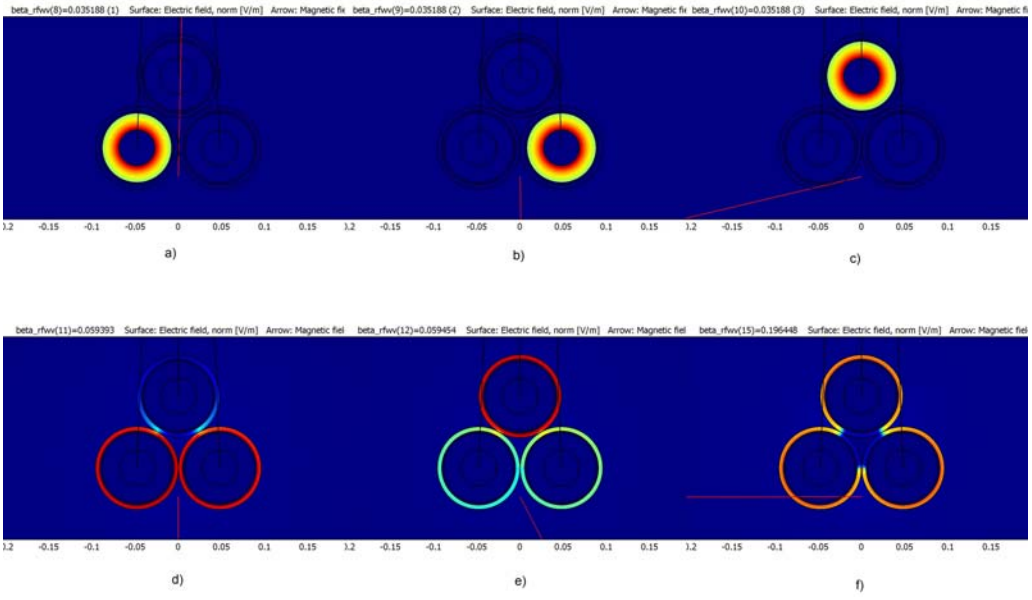

Fig. 4.50: Electric field for different modes of operation in the three cable system. They are: a) coaxial mode 1, b) coaxial mode 2, c) coaxial mode 3, d) inter sheath mode 1, e) inter sheath mode 2, and f) ground mode.

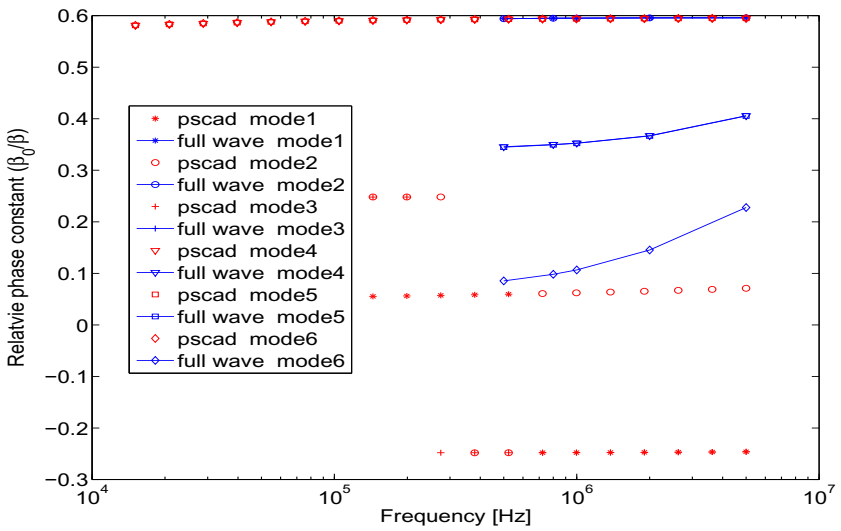

Fig. 4.51: Relative phase constant of the three cable system.

Same as the two cable system, all the coaxial modes gives identical propagation (Fig. 4.51) and attenuation constants (Fig. 4.52). In both method, the values are same. Two intersheath modes gives almost same β and α in each method. But, when compared between the methods, two methods gives different values for different frequencies. β for ground modes seems like converging at lower frequencies in two methods of calculation. But the values are different at higher frequencies for two methods. In full wave method, the rate of change in both attenuation and propagation constant increases at higher frequencies. We also find the problem of mode switching and negative beta for PSCAD calculation.

As in Fig. 4.53 and 4.54, at higher frequencies the rate of change in the per unit length resistance is lower in full wave method when compared to PSCAD.

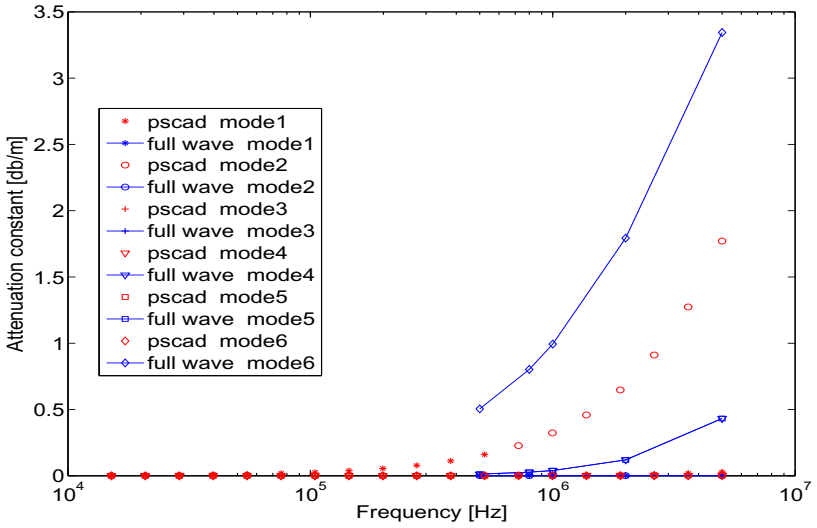

Fig. 4.52: Attenuation constant of the three cable system.

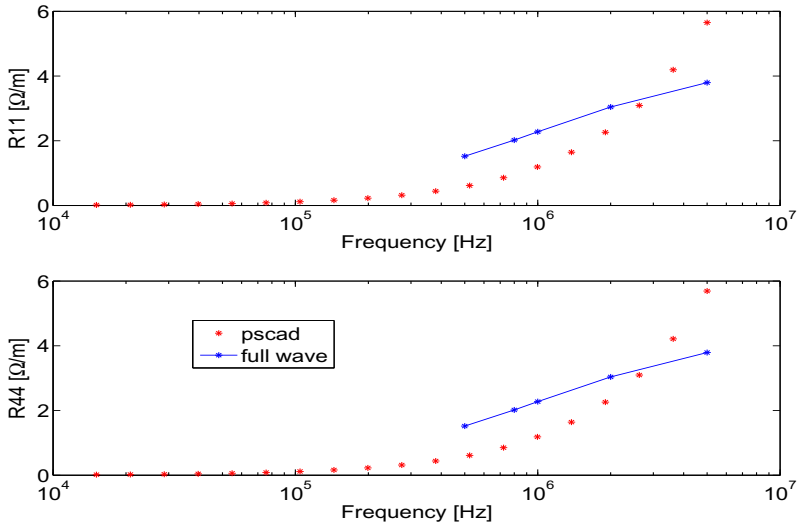

Fig. 4.53: Diagonal elements of per unit length resistance matrix of the three cable system.

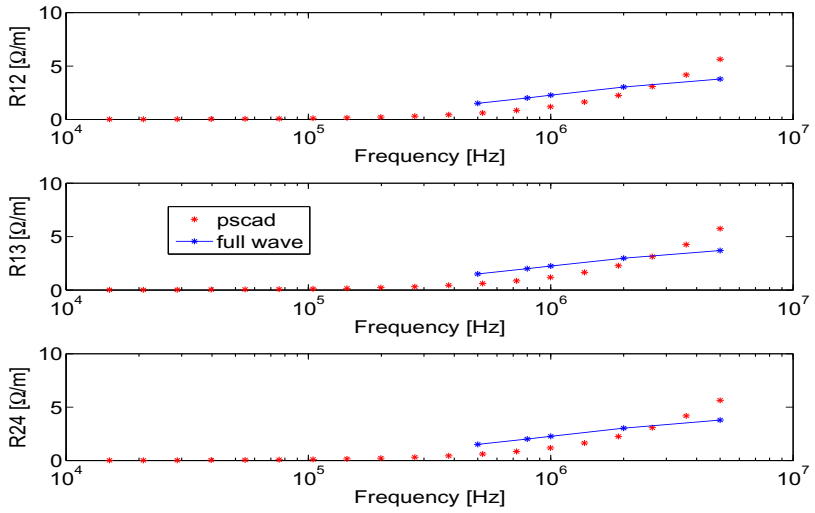

Fig. 4.54: Off diagonal elements of per unit length resistance matrix of the three cable system.

Full wave method gives lower per unit length self (Fig. 4.55) and mutual (Fig. 4.56) inductances at the higher frequencies. But the rate the inductances are changing with frequencies are similar in two methods.

PSCAD gives fixed values (Fig. 4.57) for all the components of the capacitance matrix and for all the frequencies. In full wave the per unit length capacitance component between the sheaths decreases with frequencies. The other elements are either very small (almost zero) or fixed and matches with PSCAD values.

4.5 A Sector Shaped Cable System with Four Conductors

One very important advantage about the proposed method is that, it is capable of analyzing cables with any shape. Process would be same for any cable. To

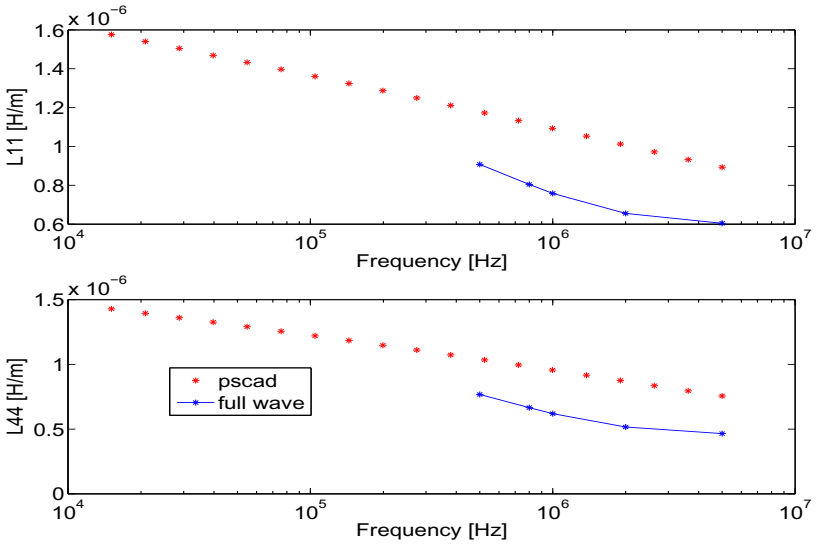

Fig. 4.55: Per unit length self inductance of the three cable system.

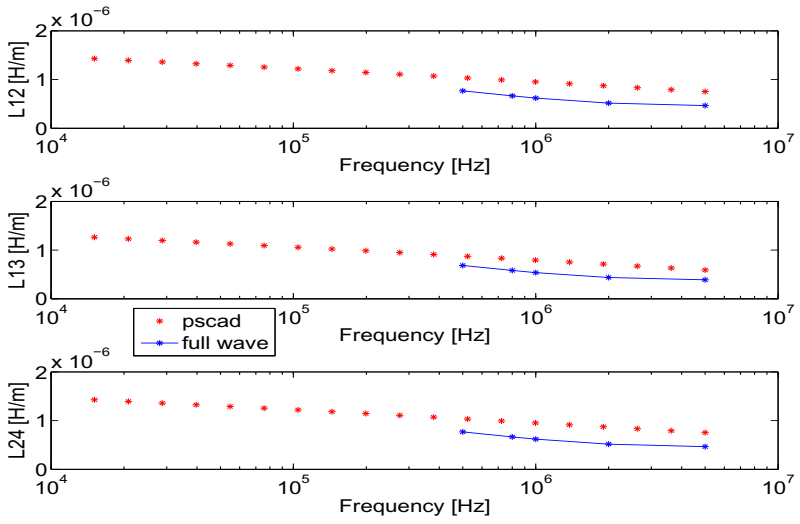

Fig. 4.56: Per unit length mutual inductance of the three cable system.

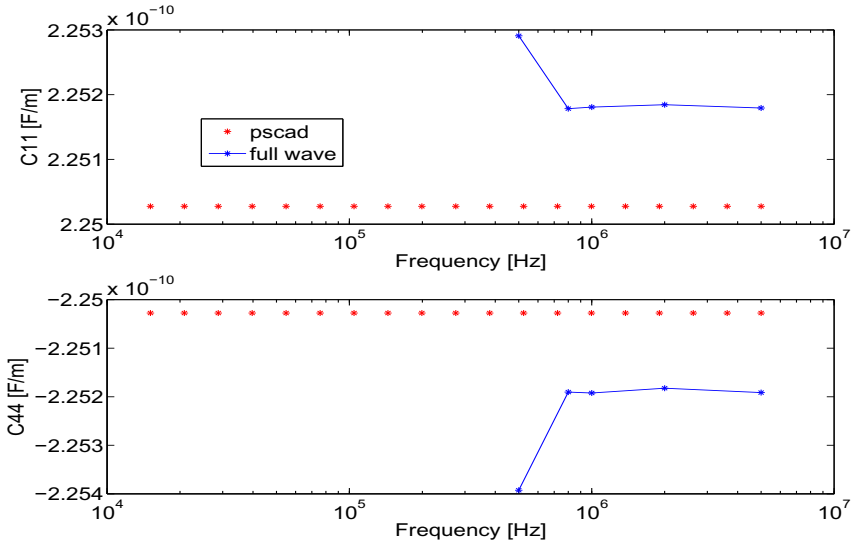

Fig. 4.57: Per unit length self capacitance of the three cable system.

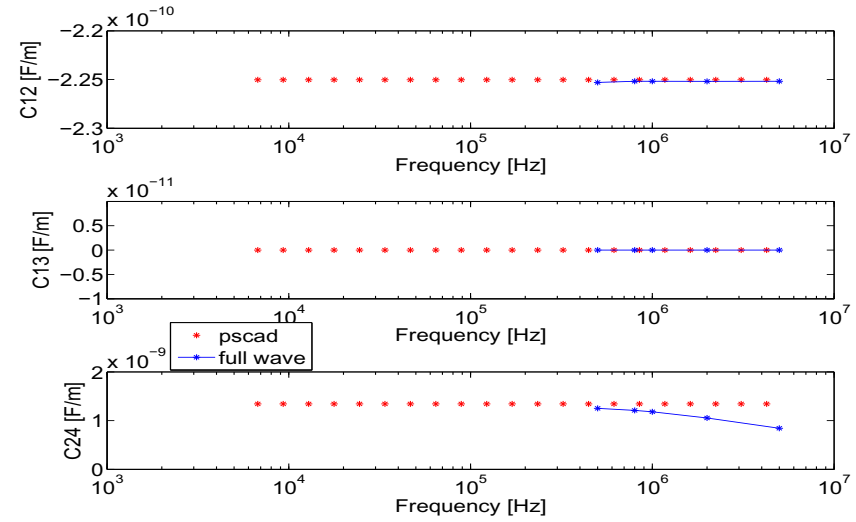

Fig. 4.58: Per unit length mutual capacitance of the three cable system.

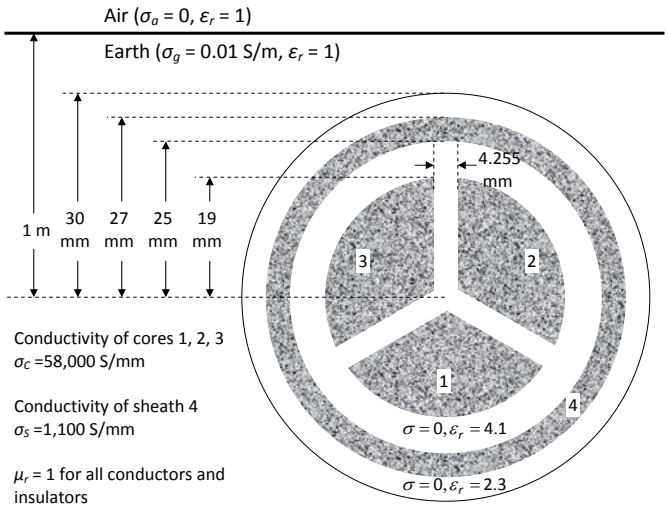

Fig. 4.59: Cross sectional geometry of a sector shaped cable. Dimensions are adopted from [2].

demonstrate that, a sector shaped cable was chosen from [2] and [20]. The cable has three sector shaped cores and they are surrounded by a sheath. The cable is placed in ground at a depth of 1m. The dimensions of the cable is given in Fig. 4.59.

From Fig. 4.61 we can see that three out of four modes have identical propagation and attenuation constants. In two of these modes (Figure 4.60), the current flows only through the cores. In the third mode, the current flows through three core and comes back through the sheath. The propagation constants for these modes are not much effected by change in frequencies. And the attenuation is almost constant for these modes. But the fourth mode is the ground mode where the current flows through sheath and comes back through ground. This mode is significantly affected by change in frequencies. The rate of change in both propagation

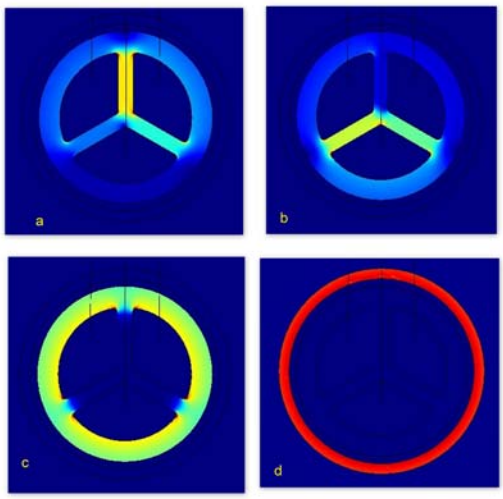

Fig. 4.60: Electric field distribution for a four conductor sector shaped cable for four modes of operation. They are: a) inter core mode 1, b) inter core mode 2, c) coaxial mode, and d) ground mode.

and attenuation constants increases with increase in frequency.

As in Fig. 4.62, we observe that the per unit length resistance is not affected with change in frequency. But both per unit length self and mutual inductances are changing with frequencies. The per unit length mutual capacitance is not changing as well (Fig. 4.63). The only element in capacitance matrix that is affected by the frequencies are the self capacitance of the sheath. The same phenomenon was observed in circular cables.

The same sector shaped cable, with no ground, has been simulated by using the partial subconductor equivalent circuit (PSEC) method [2], [37]. The values of the self and mutual resistance and inductance obtained using the PSEC method and the full wave method (at 500kHz) are compared in Table 4.3. This comparison

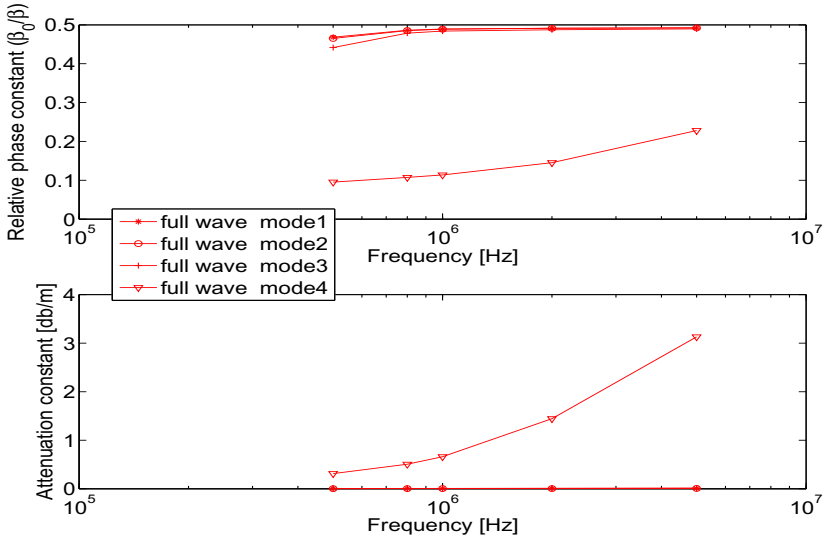

Fig. 4.61: Relative phase and attenuation constant of a sector shaped cable system.

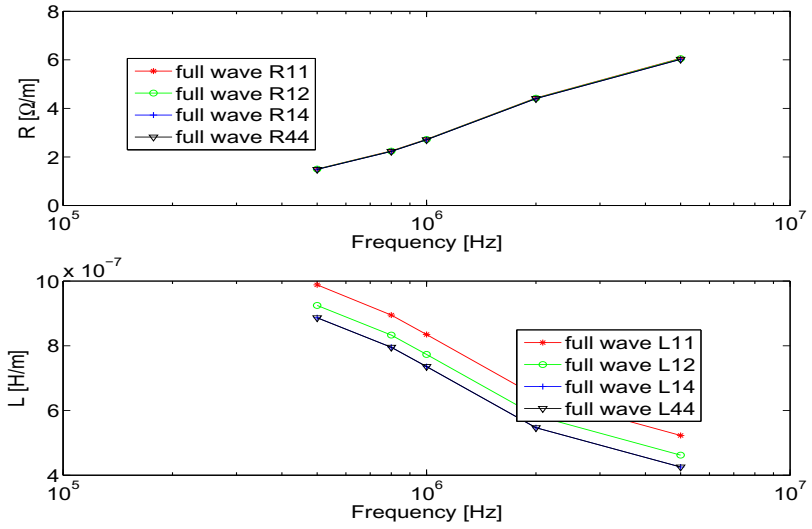

Fig. 4.62: Per unit length resistance and per unit length inductance of a sector shaped cable system.

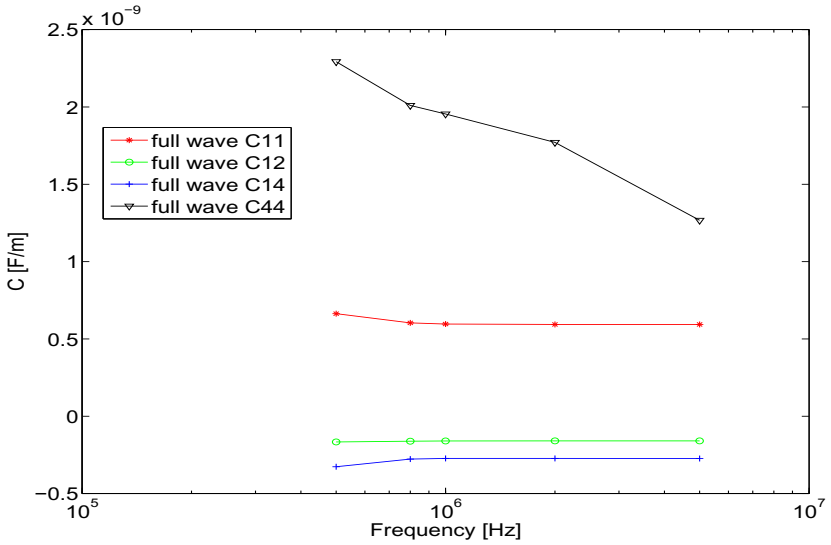

Fig. 4.63: Per unit length capacitance of a sector shaped cable system.

Tab. 4.3: Comparison Between PSEC and full wave method at 500kHz when the sector shaped cable is simulated without ground.

Method	$R_{self}(ohm/km)$	$R_{mutual}(ohm/km)$	$L_{self}(\mu\text{H/km})$	$L_{mutual}(\mu\text{H/km})$
PSEC	14	8	105	40
Full wave	13.87	8.1	100.2	38.3

shows a good agreement between the methods. Full wave modal analysis technique is also able to evaluate the per unit length capacitance. But PSEC method does not give capacitance value. The self and mutual capacitances for the sector shaped cable of [2] are 614 and 169.66 nF/km, respectively.

4.6 Proximity and Skin Effect

Both proximity and skin effects can be very important when high frequency signal is considered. Both effects are included in the proposed method. To demonstrate

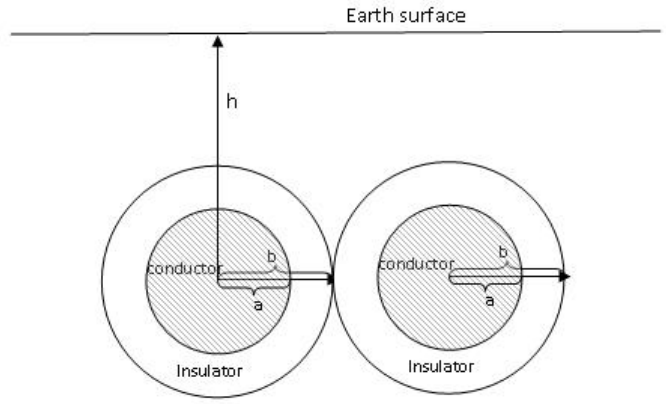

Fig. 4.64: A two cable system with two conductors, where, each cable consists of a core/conductor only. h is the burial depth of the cable. Radius a and b are given in Table 4.4.

that we have used a very simplified case. We selected a two cable system with two conductors (Fig. 4.64), where, each cable has no sheath. It has only a conductor and a insulator. The parameters are given in the Table. 4.4. For demonstration we choose the frequency as 10kHz.

We have two modes of operation. One mode can be termed as differential mode (inter conductor mode), where the current goes through one of them and then comes back through the other. Second mode can be termed as common mode (ground mode), where the current goes through two of them and comes back through the ground. In inter conductor mode, the direction of the currents are opposite inside two conductors. So, current density is higher in the nearest region of the conductors. Fig. 4.65 shows the normalized absolute value of current density for the case. In Fig. 4.66, normalized absolute current density along a cross sectional line, passed through the center of the conductors, is shown.

Tab. 4.4: Parameters used for the two cable system with two conductors

a	2 cm
b	2.5 cm
wire conductivity	$1 \times 10^6 S/m$
wire relative permittivity	1
wire relative permeability	1
insulator conductivity	0
insulator relative permittivity	3
insulator relative permeability	1
ground conductivity	$1 S/m$
ground relative permittivity	1
ground relative permeability	1
h	1 m

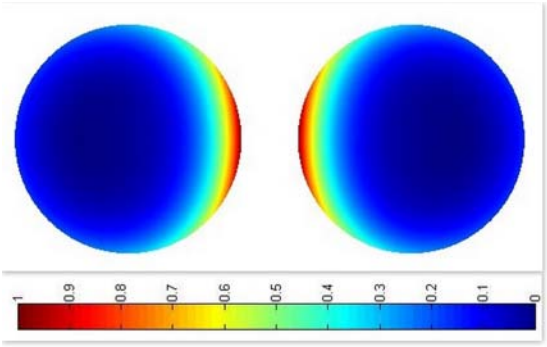

Fig. 4.65: Normalized absolute value of current density inside the two cable system with two conductors for differential mode of operation.Due to proximity effect, current density is more in the nearest region of two conductors.

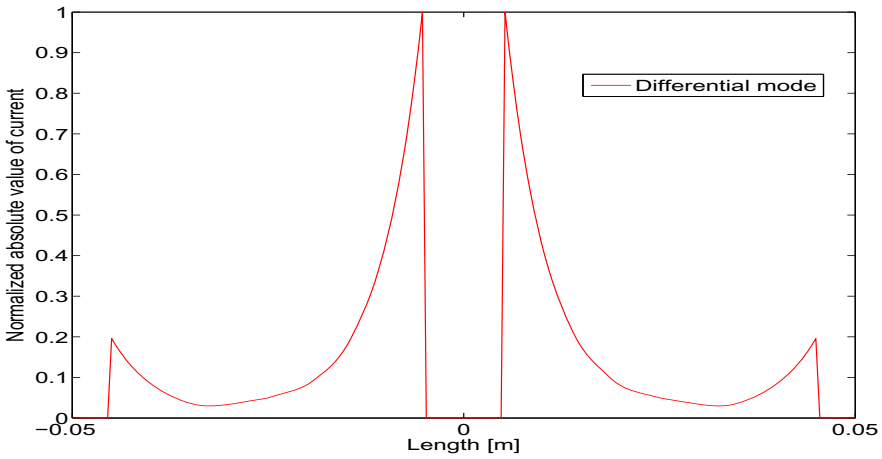

Fig. 4.66: Normalized absolute value of current density along the cross section line passed through the center of the two conductors. It shows very high current density in the region where two conductors have least distance among themselves. The current flows through one of the conductor and returns through the other.

On the other hand, in case of common mode, the conductor current flows in the same direction. So, the current density is higher in farthest region. Fig. 4.67 shows the normalized absolute value of current density of this mode and Fig. 4.68 shows the normalized absolute value of current density along a line passed through the center of the conductors. In both case, we can see the skin effect as well. Currents are flowing near the surface of the conductors.

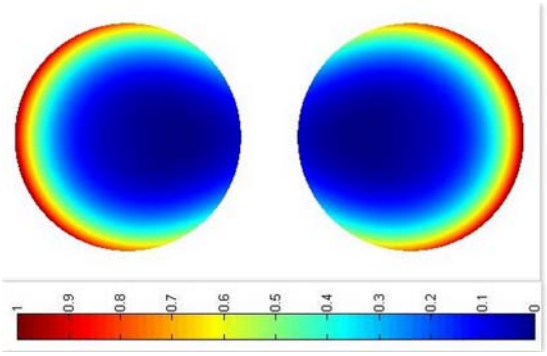

Fig. 4.67: Normalized absolute value of current density inside the two cable system with two conductors for common mode of operation. Due to proximity effect, current density is more in the farthest region of two conductors.

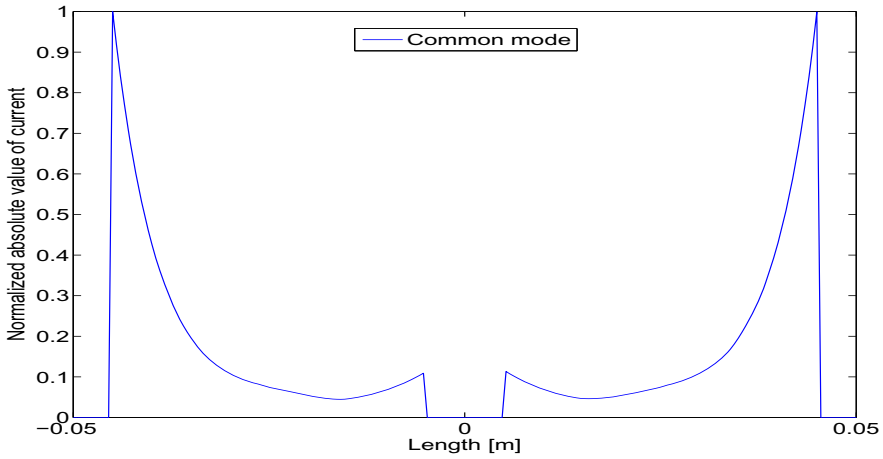

Fig. 4.68: Normalized absolute value of current density along the cross section line passed through the center of the two conductors. It represents the common mode of operation. It shows very high current density in the farthest region of two conductors. Currents flow at the same direction inside the conductors.

5. TIME DOMAIN SIMULATION

5.1 Time Domain Simulation of A Single Cable System with Two Conductors

We have calculated the impedance and admittance using the full wave method and used it for time domain simulation. As seen in the last chapter (Figs. 4.27, 4.28 and 4.29), at lower frequencies, the data from full wave method and PSCAD are converging. So, for lower frequencies, we have used Z and Y components from PSCAD. For frequencies higher than 500kHz, we used the Z and Y, calculated using the full wave method. We compared it with the result from PSCAD. Here, we are giving example for a single cable with sheath and conductor. The dimensions are same as given in Fig. 4.23. The cable parameters are also same as given in Table 4.2. This is a two conductors transmission line. So, there are two modes of operation. In differential mode (also termed as coaxial mode) of operation, the current goes through the conductor and comes back through the sheath. In common mode (also termed as ground mode or sheath mode) of operation, the current goes both through conductor and sheath and comes back through the

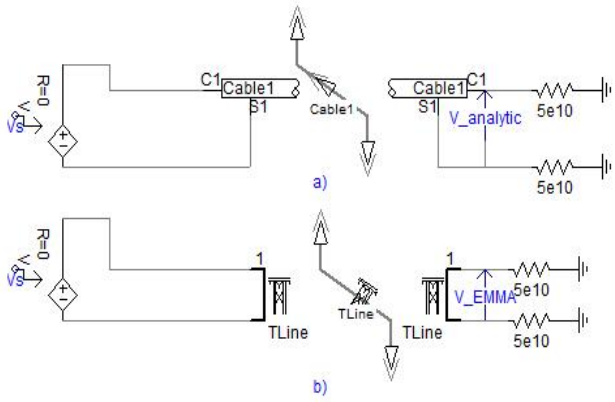

Fig. 5.1: Circuit for differential mode of operation for the single cable system with two conductors.

ground.

5.1.1 Differential Mode of Operation

As we observed in previous chapter (Fig. 4.25, Fig. 4.26), the propagation constants match closely for full wave method and PSCAD when differential mode is considered. We can see this effect in time domain simulation as well.

The circuit for differential mode of operation are given in Fig. 5.1. At first, lightning pulse is used as the excitaion, which contains frequency signal component upto 1MHz [38]. The results are given in Fig. 5.2. Both the outputs match closely with each other.

Switching pulse contains lower frequency content compared to lightning pulse. So when the circuit is excited with the switching pulse, the output from both method should match as we can see from Fig. 5.3.

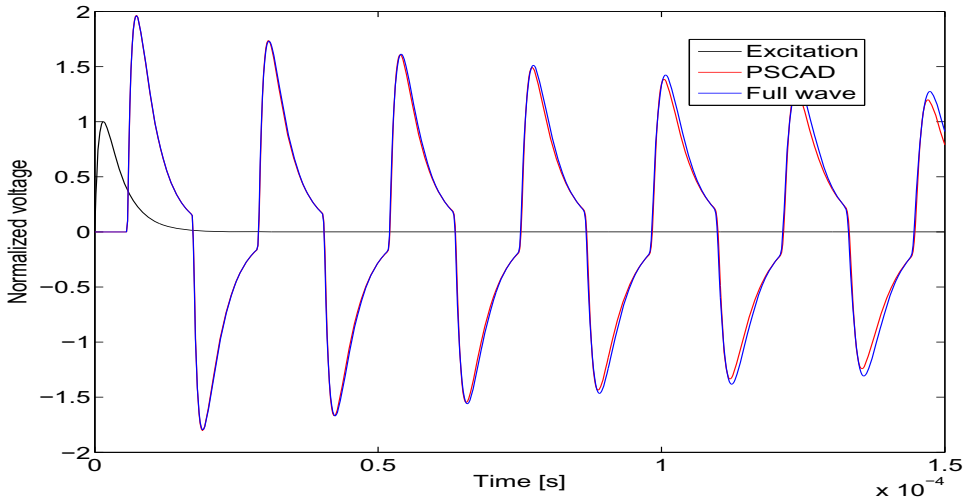

Fig. 5.2: Time domain simulation for differential mode of operation for the single cable system with two conductors. In this case, a $1.2/5\mu s$ lightning pulse is used as excitation.

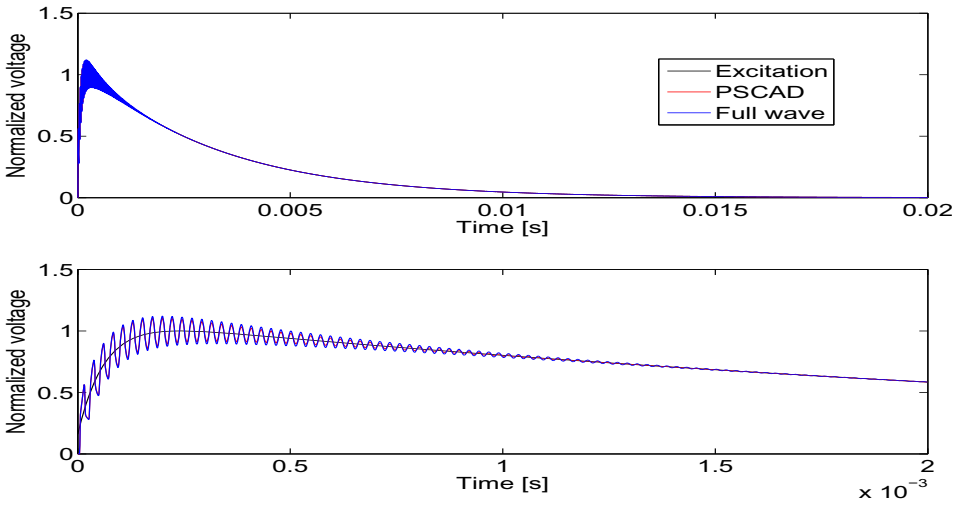

Fig. 5.3: Time domain simulation for differential mode of operation for the single cable system with two conductors with a $250/2500\mu s$ switching pulse, used as the excitation. Second figure is the zoomed version of first figure.

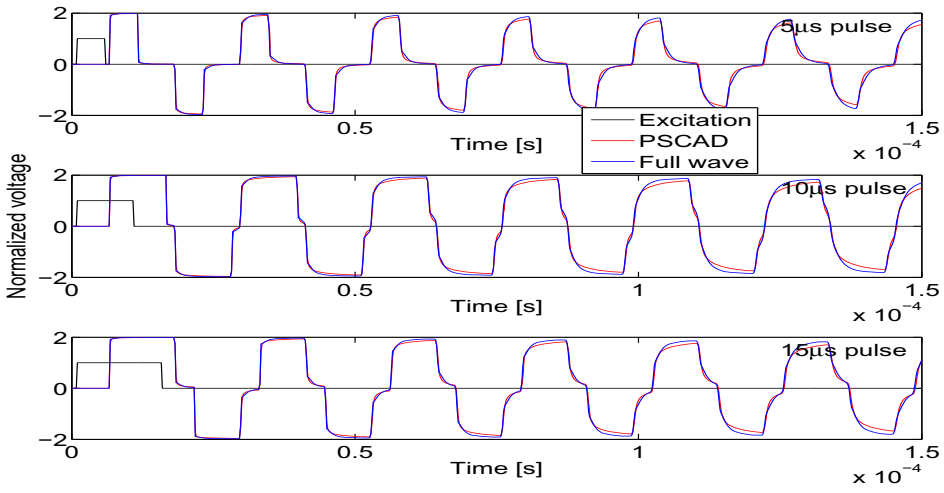

Fig. 5.4: A square pulse response of differential mode of operation for the single cable system with two conductors. Three different widths are assumed for the square pulse; $5\mu s$, $10\mu s$, and $15\mu s$.

Square pulse signal of three different widths ($5\mu s$, $10\mu s$, and $15\mu s$) are also used to observe the effect for higher frequency operations. In differential mode of operation, both methods gives very close output as seen in Fig. 5.4. As both the phase and attenuation constants, from both methods, match in this mode for all frequencies, the time domain results also match.

5.1.2 Common Mode of Operation

Fig. 5.5 shows circuit for common mode of operation. In this mode of operation, both the phase and attenuation constants at higher frequencies are different for two methods. But at lower frequencies the propagation constants are same. So, when

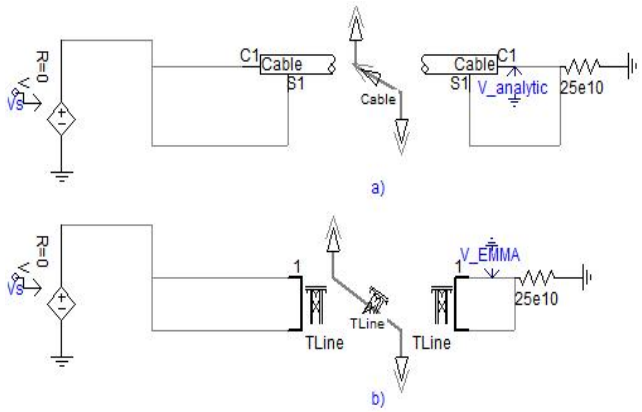

Fig. 5.5: Circuit for common mode of operation for the single cable system with two conductors.

we use lightning pulse (with higher frequencies signal components) as excitation signal, the outputs from two methods are considerably different (Fig. 5.6). Switching pulse consists of lower frequency components when compared with the lightning pulse. If switching pulse is used as the excitation then the outputs from both methods are close. (Fig. 5.7). Though they are different at the beginning (Fig. 5.7). We also studied the square pulse response of this mode of operation as seen in Fig. 5.8. As higher frequency components are included in this pulse, outputs from two methods are significantly different.

In common mode of operation, if the excitation signal contains higher frequency (larger than 500kHz) components, both the speed and attenuation of the output signals are different in two methods.

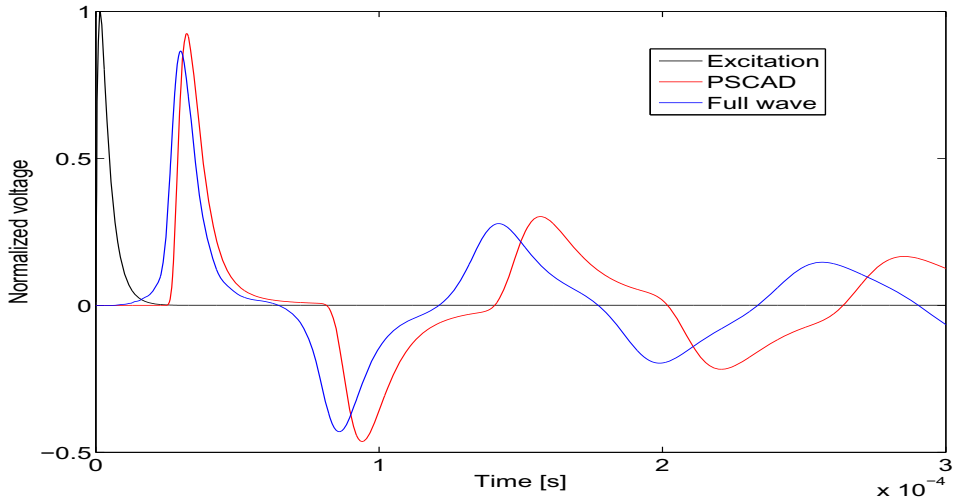

Fig. 5.6: Time domain simulation for common mode of operation for the single cable system with two conductors. In this case, a $1.2/5\mu s$ lightning pulse is used as the excitation.

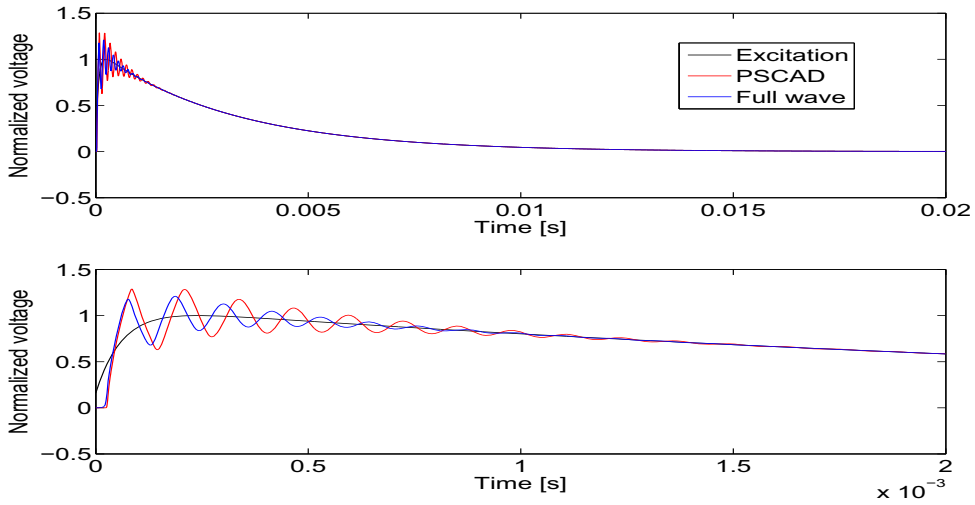

Fig. 5.7: Time domain simulation for common mode of operation for the single cable system with two conductors with a $250/2500\mu s$ switching pulse. Second figure is the zoomed version of first figure.

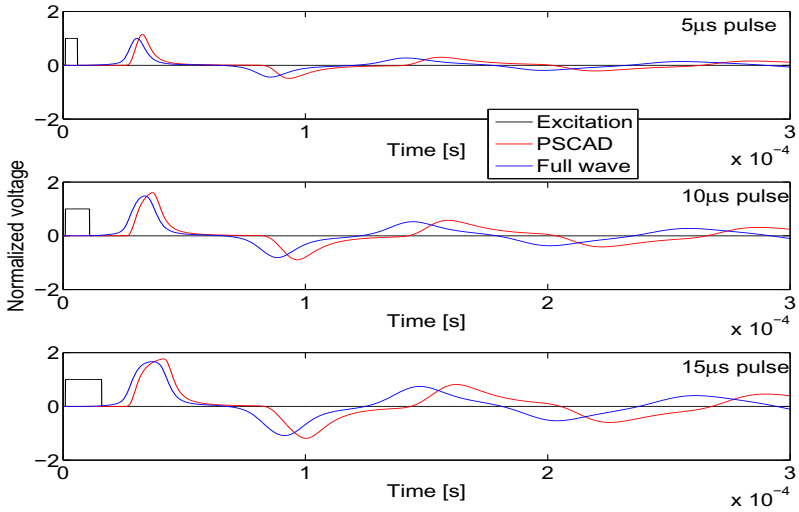

Fig. 5.8: A square pulse response of differential mode of operation for the single cable system with two conductors. Three different widths are assumed for the square pulse; $5\mu s$, $10\mu s$, and $15\mu s$.

6. CONCLUDING REMARKS

6.1 Overview

In this thesis, a full wave modal analysis technique has been introduced for the calculation of frequency-dependent per unit length parameters of underground cables buried in lossy earth. Different approaches can be found in literature for calculating these parameters. But there are some kind of limitation in each of them. Some approach is capable of calculating parameters only for coaxial cables, some approach cannot calculate admittance matrix, some method makes approximation for calculation of ground impedance and some of them are limited to a certain range of frequencies. We have discussed those in details in first chapter. Full wave method, discussed in this thesis, can overcome all the limitations mentioned previously. We have studied this method for frequencies upto 5MHz. It can be done for higher frequencies. For higher frequencies, we need to make the mesh size finer, which will require more computer memory and computation time.

The proposed method is capable of simulating cables of any shape. It is also not limited by the number of conductors. Skin effect and proximity effect are consid-

ered in the calculation of the per unit length impedance and admittance matrices.

We studied several examples in this thesis. A single coaxial cable system with one conductor, a single coaxial cable system with two conductors, two coaxial cable system with four conductors, three coaxial cable system with six conductors and a four conductor sector shaped cable were studied. We have also included some parametric studies where the effect of cable burial depth, wire conductivity, wire permittivity, ground conductivity, ground permittivity and distance between two cables have been reviewed. We compared the results with those obtained from other techniques and formulations.

Proximity effect can be very important for cable simulation at higher frequencies. We have demonstrated with a simple example that both proximity and skin effects are considered in the full wave method.

The full wave modal analysis is not practical at low frequencies. Because, at these frequencies the propagation constants of the modes are very close and it is not easy to distinguish them from each other. However, at low frequencies, the quasi-static formulation is very accurate and can be used.

The results from our method can be implemented in EMTP like programs.

Time domain simulation of the cable using the parameters calculated by full wave method clearly different from the time domain simulation of PSCAD model when common mode operation is concerned at high frequencies. In case of differential mode operation, the results matches with those from conventional programs. Theoretically, proximity effect is high in common mode of operation which leads to the difference in time domain results.

The results from this method can be used as bench mark as no approximation has be made during calculation.

6.2 Future Works

In all of our examples, we have selected zero conductivity for the insulators. So conductances calculated was zero. But in real life situation, there are layers of semiconductor material in underground cables. In future, this method can be extended to see the effect of those semiconductor material in impedance and admittance matrices.

We have demonstrated the time domain simulation for a single cable with two conductors. In future, same method can be extended for more complex cable system. Some benchmark results are found in literatures, where measurements are included for different cable system. In future those cable system can be modeled to verify the time domain results with their benchmark results.

REFERENCES

[1] L. M. Wedepohl and D. J. Wilcox, "Transient analysis of underground power-transmission systems," *IEE Proceedings*, vol. 120, no. 2, 1973.

[2] R. Rivas and J. Marti, "Calculation of frequency-dependent parameters of power cables: matrix partitioning techniques," *IEEE Transactions on Power Delivery*, vol. 17, no. 4, pp. 1085 – 1092, Oct. 2002.

[3] A. Ametani, "Wave propagation characteristics of cables," *IEEE Transactions on Power Apparatus and Systems*, vol. PAS-99, no. 2, pp. 499–505, March/April 1980.

[4] N. Nagaoka and A. Ametani, "Transient calculations on crossbonded cables," *Power Apparatus and Systems, IEEE Transactions on*, vol. PAS-102, no. 4, pp. 779 –787, 1983.

[5] L. Marti, "Simulation of transients in underground cables with frequency-dependent modal transformation matrices," *Power Delivery, IEEE Transactions on*, vol. 3, no. 3, pp. 1099 –1110, Jul. 1988.

[6] A. Morched, B. Gustavsen, and M. Tartibi, "A universal model for accurate calculation of electromagnetic transients on overhead lines and underground cables," *IEEE Transactions on Power Delivery*, vol. 14, no. 3, pp. 1032–1038, July 1999.

[7] F. Uribe, "Assessing closed-form approximations for underground cable earth impedances," in *Power Engineering Society General Meeting, 2003, IEEE*, vol. 2, 2003, p. 4 vol. 2666.

[8] B. Gustavsen, J. Sletbak, and T. Henriksen, "Simulation of transient sheath overvoltages in the presence of proximity effects," *IEEE Transactions on Power Delivery*, vol. 10, no. 2, pp. 1066 –1075, Apr. 1995.

[9] U. Gudmundsdottir, J. De Silva, C. Bak, and W. Wiechowski, "Double layered sheath in accurate hv xlpe cable modeling," in *Power and Energy Society General Meeting, 2010 IEEE*, 2010, pp. 1 –7.

[10] U. Gudmundsdottir, B. Gustavsen, C. Bak, W. Wiechowski, and F. d. Silva, "Field test and simulation of a 400 kv crossbonded cable system," *IEEE Transactions on Power Delivery*, unpublished, manuscript submitted in October 2009.

[11] U. Gudmundsdottir, C. Bak, W. Wiechowski, and F. d. Silva, "Wave propagation and benchmark measurements for cable model validation," *IEEE Transactions on Power Delivery*, unpublished, manuscript submitted in November 2009.

[12] U. Gudmundsdottir, *Modelling of long High Voltage AC Cables in the Transmission System.* Department of Energy Technology, Aalborg University, 2010.

[13] [Online]. Available: http://www.europacable.com/default.aspx?ident_id=82rubrikID=6

[14] J. Arrilaga and N. R. Watson, *Power System Harmonics*, 2nd ed. John, 2003.

[15] *1100-1992 (Emerald Book) IEEE Recommended Practice for Powering and Grounding Sensitive Electronic Equipment*, ANSI Std.

[16] A. Imece, D. W. Durbak, H. Elahi, S. Kolluri, A. Lux, D. Mader, and et all, "Modeling guidelines for fast front transients -report prepared by the fast front transient task force of the ieee modeling and analysis of system transients working group," *IEEE Transactions on Power Delivery*, vol. 11, pp. 493 – 506, 1996.

[17] H. De Paula, M. Chaves, D. Andrade, J. Domingos, and M. Freitas, "A new strategy for differential overvoltages and common-mode currents determination in pwm induction motor drives," in *Electric Machines and Drives, 2005 IEEE International Conference on*, May 2005, pp. 1075 –1081.

[18] C. Paul, *Analysis of multiconductor transmission lines.* Wiley-Interscience, 2008.

[19] A. Ametani, "A general formulation of impedance and admittance of cables," *IEEE Transactions on Power Apparatus and Systems*, vol. PAS-99, no. 3, pp. 902 –910, May 1980.

[20] A. Ametani and I. Fuse, "Approximate method for calculating the impedances of multiconductors with cross sections of arbitrary shapes," *Electrical Engineering in Japan*, vol. 112, no. 2, pp. 117–123, 1992.

[21] P. de Arizon and H. W. Dommel, "Computation of cable impedances based on subdivision of conductors," *IEEE Transactions on Power Delivery*, vol. 2, no. 1, pp. 21 –27, 1987.

[22] S. Lucas, Robert; Talukdar, "Advances in finite element techniques for calculating cable resistances and inductances," *IEEE Transactions on Power Apparatus and Systems*, vol. PAS-97 Issue:3, pp. 875 – 883, May 1978.

[23] J. Dickinson and P. Nicholson, "Calculating the high frequency transmission line parameters of power cables," in *ISPCLA ESSEN*, April 1997, pp. 127–133.

[24] K. K. M. A. Kariyawasam, A. M. Gole, and B. Kordi, "Accurate electromagnetic transient modelling of sector-shaped cables," in *International Conference on Power Systems Transients*, 2011.

[25] Y. Yin and H. Dommel, "Calculation of frequency-dependent impedances of underground power cables with finite element method," *IEEE Transactions on Magnetics*, vol. 25, no. 4, pp. 3025 –3027, Jul. 1989.

[26] S. Cristina and M. Feliziani, "A finite element technique for multiconductor cable parameters calculation," *IEEE Transactions on Magnetics*, vol. 25, no. 4, pp. 2986 –2988, Jul. 1989.

[27] A. Darcherif, A. Raizer, G. Meunier, J. Imhoff, and J. Sabonnadiere, "New techniques in fem field calculation applied to power cable characteristics computation," *IEEE Transactions on Magnetics*, vol. 26, no. 5, pp. 2388 –2390, Sep. 1990.

[28] G. Papagiannis, D. Tsiamitros, G. Andreou, D. Labridis, and P. Dokopoulos, "Earth return path impedances of underground cables for the multi-layer case: a finite element approach," in *Power Tech Conference Proceedings, 2003 IEEE Bologna*, June 2003.

[29] F. Pollaczek, "Uber die induktionswirkungen einer wechelstromeinfachleitung," *Electrishe Nachrichten Technik*, vol. 4, no. 1, pp. 18–30, 1927.

[30] O. Saad, G. Gaba, and M. Giroux, "A closed-form approximation for ground return impedance of underground cables," *IEEE Transactions on Power Delivery*, vol. 11, no. 3, pp. 1536 –1545, Jul. 1996.

[31] E. D. Sunde, *Earth conduction effects in transmission systems.* Dover Publications (New York), 1968.

[32] N. Theethayi, R. Thottappillil, M. Paolone, C. Nucci, and F. Rachidi, "External impedance and admittance of buried horizontal wires for transient studies

using transmission line analysis," *IEEE Transactions on Dielectrics and Electrical Insulation*, vol. 14, no 3, p. 751, 2007.

[33] J. R. Wait, "Electromagnetic wave propagation along a buried insulated wire," *Can. J. Phys.*, vol. 50, pp. 2402–2409, 1972.

[34] E. Petrache, F. Rachidi, M. Paolone, C. A. Nucci, V. A. Rakov, and M. A. Uman, "Lightning induced disturbances in buried cables - part i: Theory," 2005.

[35] N. Theethayi, "Electromagnetic interference in distributed outdoor electrical systems, with an emphasis on lightning interaction with electrified railway network," Ph.D. dissertation, Uppsala University2005.

[36] H. W. Dommel, *Electromagnetic Transients Program (EMTP theory book)*. Bonneville Power Administration, 1986.

[37] R. Rivas, "Calculation of frequency-dependant parameters of power cables with digital imaging and partial subconductors." Ph.D. dissertation, Department of Electrical and Computer Engineering, University of British Columbia, July, 2001.

[38] W. Kuffel, E.; Zaengl and J. Kuffel, *High Voltage Engineering Fundamentals*, 2nd ed. Butterworth-Heinemann, 2000.